Journal of Quantitative Spectroscopy & Radiative Transfer 107 (2007) 236–262

Journal of Quantitative Spectroscopy & Radiative Transfer

www.elsevier.com/locate/jqsrt

Stochastic radiative transfer model for mixture of discontinuous vegetation canopies

Nikolay V. Shabanov[a,*], D. Huang[b], Y. Knjazikhin[a], R.E. Dickinson[c], Ranga B. Myneni[a]

[a]*Department of Geography, Boston University, 675 Commonwealth Avenue, Boston, MA 02215, USA*
[b]*Brookhaven National Laboratory, Environmental Sciences Department, P.O. Box 5000, Upton, NY 11973, USA*
[c]*School of Earth and Atmospheric Sciences, Georgia Institute of Technology, Atlanta, GA 30332, USA*

Received 30 October 2006; received in revised form 15 January 2007; accepted 16 January 2007

Abstract

Modeling of the radiation regime of a mixture of vegetation species is a fundamental problem of the Earth's land remote sensing and climate applications. The major existing approaches, including the linear mixture model and the turbid medium (TM) mixture radiative transfer model, provide only an approximate solution to this problem. In this study, we developed the stochastic mixture radiative transfer (SMRT) model, a mathematically exact tool to evaluate radiation regime in a natural canopy with spatially varying optical properties, that is, canopy, which exhibits a structured mixture of vegetation species and gaps. The model solves for the radiation quantities, direct input to the remote sensing/climate applications: mean radiation fluxes over whole mixture and over individual species. The canopy structure is parameterized in the SMRT model in terms of two stochastic moments: the probability of finding species and the conditional pair-correlation of species. The second moment is responsible for the 3D radiation effects, namely, radiation streaming through gaps without interaction with vegetation and variation of the radiation fluxes between different species. We performed analytical and numerical analysis of the radiation effects, simulated with the SMRT model for the three cases of canopy structure: (a) non-ordered mixture of species and gaps (TM); (b) ordered mixture of species without gaps; and (c) ordered mixture of species with gaps. The analysis indicates that the variation of radiation fluxes between different species is proportional to the variation of species optical properties (leaf albedo, density of foliage, etc.) Gaps introduce significant disturbance to the radiation regime in the canopy as their optical properties constitute major contrast to those of any vegetation species. The SMRT model resolves deficiencies of the major existing mixture models: ignorance of species radiation coupling via multiple scattering of photons (the linear mixture model) or overestimation of this coupling due to neglecting spatial clumping of species (the TM approach). Thus, based on the former experience with mixture modeling, this study establishes an advanced theoretical basis for future mixture applications.

Keywords: Radiative transfer; 3D effects; Vegetation structure; Mixture modeling

*Corresponding author. Tel.: +1 617 353-5985; fax: +1 617 353 8399.
E-mail address: shabanov@bu.edu (N.V. Shabanov).

0022-4073/$ - see front matter © 2007 Elsevier Ltd. All rights reserved.
doi:10.1016/j.jqsrt.2007.01.053

1. Introduction

Natural vegetation exhibits significant degree of spatial heterogeneity, which complicates retrieval of the Earth's land biophysical parameters from remote sensing observations. Advances in remote sensing technology, including improved geolocation, sensor optics calibration, atmospheric correction, multi-resolution, multi-spectral and multi-angular measurements, etc., provide better means to capture land surface heterogeneity. In fact, current suite of NASA's MODerate resolution Imaging Spectroradiometer (MODIS) land products already includes a product, which explicitly characterizes mixture of land cover types—vegetation continuous fields (WWW1: Vegetation continuous fields product from MODIS, http://glcf.umiacs.umd.edu/data/modis/vcf/ [1]).

The problem of mixture of vegetation species is known in remote sensing as a scaling issue, that is, given biophysical parameters and radiation field over pure species at sub-pixel scale, one needs to estimate those parameters at the scale of a mixed pixel. Multiple approaches were developed to address the scaling issue, which can be grouped into two basic categories: empirical/statistical and physically based. The approaches from the first category are widely used for sub-pixel land cover characterization: linear mixture models [1,2], neural networks [3,4,27], Gaussian mixture discriminant analysis [5], decision trees [6] and others. The key idea of the above methods is to model satellite measured radiation over a mixed pixel as a weighted sum of the radiation fields over pure classes. Linear and non-linear models were implemented to retrieve the unknown weights, corresponding to the proportion of pure land cover classes in the mixed pixel. It was noted, however, that species in a mixture may exhibit significant degree of radiative interaction, which may bias retrievals especially in the case of linear models [7,8].

In contrast to the empirical methods, physically based approaches describe in details the physical processes of interaction of radiation with canopy at the level of elementary volume of vegetation. Optical properties of a mixture in such volume are represented as weighted average of optical properties of pure species. The radiative transfer equation (RTE) is used to model the radiation field with effective optical properties of mixed canopy. The above modeling principles were implemented, for instance, in a scaling scheme of the radiation block of the common land model (CLM) (WWW2: CLM, http://www.cgd.ucar.edu/tss/clm/distribution/clm3.0/index.html) [9] and the MODIS leaf area index (LAI) algorithm [10]. The major limitation of the above schemes is that they are based on the turbid medium (TM) mixture approximation, where canopy is represented as a mixed gas of vegetation species and gaps. With the TM approach, one major feature of the natural vegetation is missing-spatial structure of a mixture, which may substantially affect radiation regime.

This paper is aimed to advance theoretical description of the radiation regime in vegetation canopy under condition of spatial gradient of canopy optical properties. Applications in focus include the above-mentioned radiation block of CLM and the MODIS LAI algorithm. The spatial heterogeneity of a medium can be incorporated in the standard RT equation using the stochastic approach, which was originally formulated for broken clouds by Vainikko [11,12] and further developed by Kasianov [13], Titov [14] and Zuev and Titov [15]. Additional closely related theoretical study is the linear kinetic theory of stochastic mixture, developed by Pomraning [16]. In our former research [17,18], we adopted Vainikko's approach for vegetation canopy and formulated the stochastic RT (SRT) model for a single spatially discontinuous species. In the present work, we introduce a stochastic mixture radiative transfer (SMRT) model, an extension of the former model for the case of the structured composition of multiple vegetation species and gaps. While the focus of this paper is on vegetation canopy, the developed approach may be utilized in the other areas of RT, including cloud physics (independent pixel approximation), nuclear reactors (atomic mixture), and astrophysics. This paper is organized as follows. In Section 2, we review the parameterization of the 3D RT equation for the case of spatially varying optical properties. In Section 3, we present the detailed derivations of the SMRT model from the corresponding 3D RT equation. In Sections 4 and 5 we present analytical and numerical analysis of the radiation effects in a mixed canopy, as captured by the SMRT model. Concluding remarks are given in Section 6.

2. 3D RT model parameterization

Consider a heterogeneous vegetation canopy, a mixture of N different vegetation species and gaps as shown in Fig. 1 (for $N = 2$). The spatial structure of such canopy can be characterized by the indicator function of a

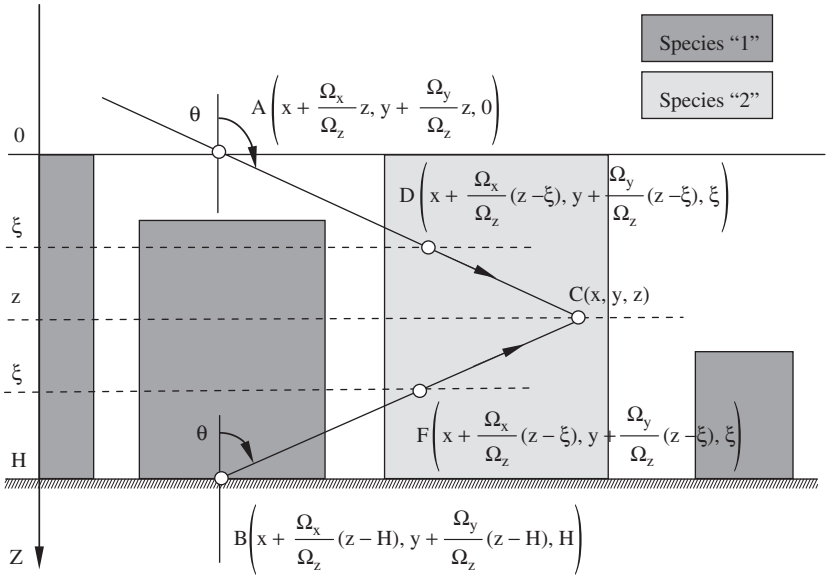

Fig. 1. Schematic plot of a mixture of discontinuous vegetation canopies (species 1 and 2) in a coordinate system. The vertical axis, z, is directed down. The angular direction, θ, is evaluated from the upward direction.

canopy, $\chi(\vec{r})$, defined for each spatial location, $\vec{r}$, as follows:

$$\chi(\vec{r}) = \sum_j \chi^{(j)}(\vec{r}), \tag{1a}$$

where $\chi^{(j)}(\vec{r})$ is an indicator function of the individual species 'j':

$$\chi^{(j)}(\vec{r}) = \begin{cases} 1, & \text{if } \vec{r} \in \text{species } j, \ j = 1, N, \\ 0, & \text{otherwise.} \end{cases} \tag{1b}$$

The equations above specify overall architecture of vegetation canopy as cumulative contribution of individual species in a mixture. The indicator function is assumed to be a random variable. We further assume that a particular spatial location is occupied only by a single species, i.e.,

$$\chi^{(i)}(\vec{r})\,\chi^{(j)}(\vec{r}) = 0, \ i \neq j.$$

Density of canopy is defined by the Leaf Area Index (LAI)—one-sided green leaf area per unit ground area (m^2/m^2). In the case of mixture of species,

$$\mathrm{LAI} = \frac{1}{S}\int_V \mathrm{d}\vec{r}\, d_{\mathrm{L}}(\vec{r}) = \sum_j \frac{1}{S}\int_V \mathrm{d}\vec{r}\, d_{\mathrm{L}}^{(j)}\,\chi^{(j)}(\vec{r}) = \sum_j \mathrm{LAI}^{(j)}, \tag{2}$$

where $d_{\mathrm{L}}^{(j)}$ and $\mathrm{LAI}^{(j)}$ are one-sided foliage area volume density (m^2/m^3) and LAI of species 'j', respectively, and the integration is performed over a volume of canopy, V, with a footprint, S. The interaction of radiation with species leaves is characterized by spatially varying extinction coefficient $\sigma(\vec{r},\vec{\Omega})$ and differential scattering coefficient, $\sigma_{\mathrm{S}}(\vec{r},\vec{\Omega}' \to \vec{\Omega})$, [19],

$$\sigma(\vec{r},\vec{\Omega}) = \sum_j \sigma^{(j)}(\vec{\Omega})\,\chi^{(j)}(\vec{r}) = \sum_j d_{\mathrm{L}}^{(j)}\,\chi^{(j)}(\vec{r})\,G^{(j)}(\vec{\Omega}), \tag{3}$$

$$\sigma_{\mathrm{S}}(\vec{r},\vec{\Omega}' \to \vec{\Omega}) = \sum_j \sigma_S^{(j)}(\vec{\Omega}' \to \vec{\Omega})\,\chi^{(j)}(\vec{r}) = \sum_j \frac{d_{\mathrm{L}}^{(j)}\,\chi^{(j)}(\vec{r})}{\pi}\,\Gamma^{(j)}(\vec{\Omega}' \to \vec{\Omega}), \tag{4}$$

where $G^{(j)}(\vec{\Omega})$ is the mean projection of leaf normals in the direction $\vec{\Omega}$ and $\Gamma^{(j)}(\vec{\Omega}' \to \vec{\Omega})$ is the area scattering phase function for species 'j' [19]. The above parameters depend on the probability density of leaf normal orientation, $g_L(\vec{r}, \vec{\Omega}_L)$, ($\vec{\Omega}_L$ is a leaf normal direction) and the spectral leaf albedo, $\omega(\vec{r}, \lambda)$ (λ is a wavelength) [19]. Given the set of structural and optical parameters, the radiation regime in a vegetation canopy is described by the following 3D transport equation for radiation intensity, $I(\vec{r}, \vec{\Omega})$:

$$\vec{\Omega} \cdot \nabla I(\vec{r}, \vec{\Omega}) + \sigma(\vec{r}, \vec{\Omega})\, I(\vec{r}, \vec{\Omega}) = \int_{4\pi} \mathrm{d}\vec{\Omega} \sigma_S(\vec{r}, \vec{\Omega}' \to \vec{\Omega})\, I(\vec{r}, \vec{\Omega}') \tag{5}$$

The unique solution of the Eq. (5) is specified by the following boundary conditions:

$$\begin{cases} I(z=0, \vec{\Omega}) = \dfrac{f_{\mathrm{dir}}(\vec{\Omega}_0)}{|\mu(\vec{\Omega}_0)|} \delta(\vec{\Omega} - \vec{\Omega}_0) + (1 - f_{\mathrm{dir}})\, \mathrm{d}(\vec{\Omega}, \vec{\Omega}_0), \mu < 0, \\ I(z=H, \vec{\Omega}) = \dfrac{\rho_{\mathrm{soil}}}{\pi} \int_{2\pi^-} I(z=H, \vec{\Omega}')\, |\mu(\vec{\Omega}')|\, \mathrm{d}\vec{\Omega}', \mu > 0, \end{cases} \tag{6}$$

where the first equation specifies incoming direct, $\delta(\vec{\Omega} - \vec{\Omega}_0)$, and diffuse, $d(\vec{\Omega}, \vec{\Omega}_0)$, radiation at the top of canopy, and f_{dir} denotes the ratio of direct to total incoming solar flux. The second equation specifies boundary condition at the canopy bottom, soil surface, which is assumed to be a Lambertian surface with hemispherical reflectance, ρ_{soil}. Note the angular integration notations: integration over the total sphere (4π), lower hemisphere ($2\pi^-$), and upper hemisphere ($2\pi^+$). To simplify numerical solution of the complete RT problem (Eqs. (5) and (6)), two sub-problems with simplified boundary conditions can be specified: (1) the BS-problem: the original illumination condition at the top of the canopy and the soil reflectance is set to 0; (2) the S-problem: there is no input energy from above, but isotropic (Lambertian) sources of energy are uniformly distributed on the canopy bottom. The solution of the complete problem can be approximated by the solutions of the S- and BS-problems as follows:

$$I(\vec{r}, \vec{\Omega}) \approx I_{\mathrm{BS}}(\vec{r}, \vec{\Omega}) + \frac{\rho_{\mathrm{soil}}}{1 - \rho_{\mathrm{soil}} R_S}\, T_{\mathrm{BS}}\, I_S(\vec{r}, \vec{\Omega}), \tag{7a}$$

$$R \approx R_{\mathrm{BS}} + \frac{\rho_{\mathrm{soil}}}{1 - \rho_{\mathrm{soil}} R_S}\, T_{\mathrm{BS}}\, T_S, \tag{7b}$$

$$A \approx A_{\mathrm{BS}} + \frac{\rho_{\mathrm{soil}}}{1 - \rho_{\mathrm{soil}} R_S}\, T_{\mathrm{BS}}\, A_S, \tag{7c}$$

$$T \approx T_{\mathrm{BS}} + \frac{\rho_{\mathrm{soil}}}{1 - \rho_{\mathrm{soil}} R_S}\, T_{\mathrm{BS}}\, R_S. \tag{7d}$$

In the equations above, I, I_{BS}, I_S denote radiation intensities, R, R_{BS}, R_S are canopy albedos, A, A_{BS}, A_S are canopy absorptances, T, T_{BS}, T_S are canopy transmittances for the complete, BS- and S-problems, respectively. The above quantities comply with the energy conservation law,

$$R + A + (1 - \rho_{\mathrm{soil}})\, T = 1, \tag{8a}$$

$$R_k + A_k + T_k = 1, \tag{8b}$$

where Eq. (8a) refers to the total problem and Eq. (8b) to two sub-problems ($k = \mathrm{S}$ or BS).

3. Formulation of the SMRT model

3.1. Basic concepts

The detailed evaluation of the 3D radiation field is computationally expensive and often unnecessary for multiple applications. Namely, in application to satellite remote sensing, radiation field, averaged over a pixel is required. The stochastic approach to the radiative transfer directly addresses the above problem, by averaging the 3D RT equation (Eq. (5)) over a horizontal plane. Thus, the average 1D equation for the

average radiation intensities is obtained. The mathematical formulation of the SRT equation requires two types of averages: (1) $U^{(i)}(z,\vec{\Omega})$, mean intensity over the portion of the horizontal plane at depth z, occupied by species 'i'; (2) $\bar{I}(z,\vec{\Omega})$, mean intensity over the total space of the horizontal plane at depth z,

$$U^{(i)}(z,\vec{\Omega}) = \lim_{R\to\infty} \frac{1}{S_R \cap T_z^{(i)}} \int \int_{S_R \cap T_z^{(i)}} \mathrm{d}x\,\mathrm{d}y \chi^{(i)}(x,y,z)\, I(x,y,z,\vec{\Omega}), \tag{9}$$

$$\bar{I}(z,\vec{\Omega}) = \lim_{R\to\infty} \frac{1}{S_R} \int \int_{S_R} \mathrm{d}x\,\mathrm{d}y I(x,y,z,\vec{\Omega}). \tag{10}$$

In the above, S_R denotes the area of a circle of radius R; $T_z^{(i)}$ denotes the area of the horizontal plane at depth z, occupied by species 'i'. The averaging procedure (cf. next Section) results in the parameterization of the resulting transfer equation in terms of two stochastic moments of a vegetation structure. The first stochastic moment is the probability, p, of finding species "i" at canopy depth z,

$$p^{(i)}(z) = \lim_{R\to\infty} \frac{1}{S_R} \int \int_{S_R \cap T_z^{(i)}} \chi^{(i)}(z,x,y)\,\mathrm{d}x\,\mathrm{d}y \equiv \lim_{R\to\infty} \frac{S_R \cap T_z^{(i)}}{S_R}. \tag{11}$$

The second moment is the pair-correlation function, q, between species 'i' at canopy depth z and species 'j' at depth ξ along the direction $\vec{\Omega}$,

$$q^{(i,j)}(z,\xi,\vec{\Omega}) = \lim_{R\to\infty} \frac{S_R \cap T_z^{(i)} \cap T_\xi^{(j)}[(\Omega_x/\Omega_z)(z-\xi),(\Omega_y/\Omega_z)(z-\xi)]}{S_R}. \tag{12}$$

In the above, Ω_x, Ω_y, and Ω_z are projections of a unit direction vector, $\vec{\Omega}$, on the x, y, and z axes, respectively. Argument for $T_\xi^{(j)}$ denotes a shift of the origin of plane ξ relative to plane z along x and y directions, required to evaluate correlation between the planes in direction $\vec{\Omega}$ (cf. Fig. 1). Using the first and second moments of a vegetation structure, the conditional pair-correlation of species, $K^{(i,j)}$, can be evaluated as

$$K^{(i,j)}(z,\xi,\vec{\Omega}) = \frac{q^{(i,j)}(z,\xi,\vec{\Omega})}{p^{(i)}(z)}. \tag{13}$$

3.2. Derivation of the SMRT equations

The approach to derive the SMRT equations for multiple species extends the one for single species [18]. The derivations start from integrating the 3D RT equation (Eq. (5)) from the upper (lower) boundary to some internal point $\vec{r}\,(x,y,z)$ along the direction $\vec{\Omega}$ (cf. Fig. 1). The resulting equation is

$$\begin{cases} I(x,y,z,\vec{\Omega}) + \frac{1}{|\mu(\vec{\Omega})|}\int_0^z \mathrm{d}\xi\sigma(\ldots,\vec{\Omega})\, I(\ldots,\vec{\Omega}) \\ \quad = \frac{1}{|\mu(\vec{\Omega})|}\int_0^z \mathrm{d}\xi \int_{4\pi} \mathrm{d}\vec{\Omega}'\sigma_S(\ldots,\vec{\Omega}'\to\vec{\Omega})\, I(\ldots,\vec{\Omega}') + I(x,y,0,\vec{\Omega}), \mu<0, \\ I(x,y,z,\vec{\Omega}) + \frac{1}{|\mu(\vec{\Omega})|}\int_z^H \mathrm{d}\xi\sigma(\ldots,\vec{\Omega})\, I(\ldots,\vec{\Omega}) \\ \quad = \frac{1}{|\mu(\vec{\Omega})|}\int_z^H \mathrm{d}\xi \int_{4\pi} \mathrm{d}\vec{\Omega}'\sigma_S(\ldots,\vec{\Omega}'\to\vec{\Omega})\, I(\ldots,\vec{\Omega}') + I(x,y,H,\vec{\Omega}), \mu>0, \end{cases} \tag{14}$$

where the following short-cut notation was used:

$$(\ldots) = \left(x + \frac{\Omega_x}{\Omega_z}(z-\xi), y + \frac{\Omega_y}{\Omega_z}(z-\xi), \xi\right). \tag{15}$$

At the next step, Eq. (14) is averaged over the total space of the horizontal plane z. The key problem at this step is to evaluate the integral terms, which involve $\sigma(\ldots,\vec{\Omega})\cdot I(\ldots,\vec{\Omega})$ and $\sigma_S(\ldots,\vec{\Omega}'\to\vec{\Omega})\cdot I(\ldots,\vec{\Omega}')$. Due to presence of the indicator function in the definition of σ and σ_S (cf. Eqs. (3) and (4)) the above integrals over the total space of the horizontal plane ξ are reduced to the integrals over the portion of the plane ξ, occupied by

all vegetation species, namely

$$T_\xi = \bigcup_j T_\xi^{(j)}. \tag{16}$$

The integral terms of interest can be evaluated by shifting the origin of T_ξ, in the x–y plane by the vector

$$\left(\frac{\Omega_x}{\Omega_z}(z-\xi), \frac{\Omega_y}{\Omega_z}(z-\xi)\right),$$

followed by separate integration over individual species (cf. Eqs. (9) and (16)):

$$\begin{aligned}
&\frac{1}{S_R}\int\int_{S_R} \mathrm{d}x\,\mathrm{d}y\sigma(\ldots,\vec{\Omega})\,I(\ldots,\vec{\Omega}) \\
&\quad = \frac{1}{S_R}\int\int_{S_R\cap T_\xi[(\Omega_x/\Omega_z)(z-\xi),(\Omega_y/\Omega_z)(z-\xi)]} \mathrm{d}x\,\mathrm{d}y\sigma(\ldots,\vec{\Omega})\,I(\ldots,\vec{\Omega}) \\
&\quad = \frac{1}{S_R}\int\int_{S'_R\cap T_\xi} \mathrm{d}x'\,\mathrm{d}y'\sigma(x',y',\xi',\vec{\Omega})\,I(x',y',\xi',\vec{\Omega}) \\
&\quad = \sum_j \frac{S_R\cap T_\xi^{(j)}}{S_R}\cdot\frac{1}{S_R\cap T_\xi^{(j)}}\int\int_{S'\cap T_\xi^{(j)}} \mathrm{d}x'\,\mathrm{d}y'\sigma^{(j)}(\vec{\Omega})\,I(x',y',\xi,\vec{\Omega}) \\
&\quad = \sum_j p^{(j)}(\xi)\cdot\sigma^{(j)}(\vec{\Omega})\,U^{(j)}(\xi,\vec{\Omega}).
\end{aligned} \tag{17}$$

Taking into account the derivations above, the equation for mean intensity over total space of horizontal plane at depth z, $\bar{I}(z,\vec{\Omega})$, is

$$\begin{cases}
\bar{I}(z,\vec{\Omega}) + \frac{1}{|\mu(\vec{\Omega})|}\sum_j \int_0^z \mathrm{d}\xi p^{(j)}(\xi)\,\sigma^{(j)}(\vec{\Omega})\,U^{(j)}(\xi,\vec{\Omega}) \\
\quad = \frac{1}{|\mu(\vec{\Omega})|}\sum_j \int_0^z \mathrm{d}\xi \int_{4\pi} \mathrm{d}\vec{\Omega}' p^{(j)}(\xi)\,\sigma_S^{(j)}(\vec{\Omega}'\to\vec{\Omega})\cdot U^{(j)}(\xi,\vec{\Omega}') + \bar{I}(0,\vec{\Omega}), \quad \mu<0, \\
\bar{I}(z,\vec{\Omega}) + \frac{1}{|\mu(\vec{\Omega})|}\sum_j \int_z^H \mathrm{d}\xi p^{(j)}(\xi)\,\sigma^{(j)}(\vec{\Omega})\cdot U^{(j)}(\xi,\vec{\Omega}) \\
\quad = \frac{1}{|\mu(\vec{\Omega})|}\sum_j \int_z^H \mathrm{d}\xi \int_z \mathrm{d}\vec{\Omega}' p^{(j)}(\xi)\,\sigma_S^{(j)}(\vec{\Omega}'\to\vec{\Omega})\,U^{(j)}(\xi,\vec{\Omega}') + \bar{I}(H,\vec{\Omega}), \quad \mu>0.
\end{cases} \tag{18}$$

In the above, $\bar{I}(0,\vec{\Omega})$ and $\bar{I}(H,\vec{\Omega})$ denote mean radiation intensities over whole horizontal plane at the canopy boundaries; in the typical case of the uniform boundary conditions they are equal to the corresponding 3D values, $I(z=0,\vec{\Omega})$ and $I(z=H,\vec{\Omega})$ (cf. Eq. (6)).

According to Eq. (18), $\bar{I}(z,\vec{\Omega})$, depends on $U^{(i)}(z,\vec{\Omega})$, $i=[1,N]$. The equations for $U^{(i)}(z,\vec{\Omega})$ can be derived by averaging Eq. (14) over the portion of a horizontal plane, occupied by species 'i'. The terms under the sign of integral in this case can be evaluated with the above-described technique (Eq. (17)), taking into account Eqs. (9), (11), (12) and (16) as follows:

$$\begin{aligned}
&\frac{1}{S_R\cap T_z^{(i)}}\int\int_{S_R\cap T_z^{(i)}} \mathrm{d}x\,\mathrm{d}y\sigma(\ldots,\vec{\Omega})\,I(\ldots,\vec{\Omega}) \\
&\quad = \frac{1}{S_R\cap T_z^{(i)}}\int\int_{S_R\cap T_z^{(i)}\cap T_\xi[(\Omega_x/\Omega_z)(z-\xi),(\Omega_y/\Omega_z)(z-\xi)]} \mathrm{d}x\,\mathrm{d}y\sigma(\ldots,\vec{\Omega})\,I(\ldots,\vec{\Omega}) \\
&\quad = \frac{1}{S_R\cap T_z^{(i)}}\int\int_{S'_R\cap T'^{(i)}_z\cap T_\xi} \mathrm{d}x'\,\mathrm{d}y'\sigma(x',y',\xi',\vec{\Omega})\,I(x',y',\xi',\vec{\Omega}) \\
&\quad = \sum_j \frac{S'_R\cap T'^{(i)}_z\cap T_\xi^{(j)}}{S_R\cap T_z^{(i)}}\,\frac{1}{S'_R\cap T'^{(i)}_z\cap T_\xi^{(j)}}\int\int_{S'_R\cap T'^{(i)}_z\cap T_\xi^{(j)}} \mathrm{d}x'\,\mathrm{d}y'\sigma^{(j)}(\vec{\Omega})\,I(x',y',\xi,\vec{\Omega})
\end{aligned}$$

$$= \sum_j \frac{q^{(i,j)}(z,\xi,\vec{\Omega})}{p^{(i)}(z)}\,\sigma^{(j)}(\vec{\Omega})\,U^{(j)}(\xi,\vec{\Omega})$$
$$\equiv \sum_j K^{(i,j)}(z,\xi,\vec{\Omega})\,\sigma^{(j)}(\vec{\Omega})\,U^{(j)}(\xi,\vec{\Omega}). \tag{19}$$

In the above derivations, we assumed that the subset $T_z^{(i)} \cap T_\xi^{(j)}$ contains the same percentage of species "j" as the total set $T_z^{(i)}$. This assumption is similar to one, introduced by Vainikko [11,12] in the derivation of the original version of stochastic equations for atmosphere. This assumption is called "local chaotisity and global order" and is required to close system of stochastic equations using only first two moments of structure. Given Eqs. (19) and (14), we can formulate equation for $U^{(i)}(z,\vec{\Omega})$ as follows:

$$\begin{cases} U^{(i)}(z,\vec{\Omega}) + \frac{1}{|\mu(\vec{\Omega})|}\sum_j \int_0^z \mathrm{d}\xi K^{(i,j)}(z,\xi,\vec{\Omega})\,\sigma^{(j)}(\vec{\Omega})\,U^{(j)}(\xi,\vec{\Omega}) \\ = \frac{1}{|\mu(\vec{\Omega})|}\sum_j \int_0^z \mathrm{d}\xi \int_{4\pi} d\vec{\Omega}' K^{(i,j)}(z,\xi,\vec{\Omega})\,\sigma_S^{(j)}(\vec{\Omega}'\to\vec{\Omega})\,U^{(j)}(\xi,\vec{\Omega}') + U^{(i)}(0,\vec{\Omega}), \quad \mu<0, \\ U^{(i)}(z,\vec{\Omega}) + \frac{1}{|\mu(\vec{\Omega})|}\sum_j \int_z^H \mathrm{d}\xi K^{(i,j)}(z,\xi,\vec{\Omega})\,\sigma^{(j)}(\vec{\Omega})\cdot U^{(j)}(\xi,\vec{\Omega}) \\ = \frac{1}{|\mu(\vec{\Omega})|}\sum_j \int_z^H \mathrm{d}\xi \int_{4\pi} \mathrm{d}\vec{\Omega}' K^{(i,j)}(z,\xi,\vec{\Omega})\,\sigma_S^{(j)}(\vec{\Omega}'\to\vec{\Omega})\,U^{(j)}(\xi,\vec{\Omega}') + U^{(i)}(H,\vec{\Omega}), \quad \mu>0. \end{cases} \tag{20}$$

In the above, $U^{(i)}(0,\vec{\Omega})$ and $U^{(i)}(H,\vec{\Omega})$ denote mean radiation intensities over the portion of horizontal plane occupied by species 'i' at the canopy boundaries; in the typical case of the uniform boundary conditions they are equal to corresponding 3D values, $I(z=0,\vec{\Omega})$ and $I(z=H,\vec{\Omega})$ (cf. Eq. (6)). Note that, in contrast to a single equation for single species [18], the Eq. (20) for N species corresponds to systems of N equations. This accounts for the fact of species radiative coupling.

3.3. Separation of direct and diffuse fluxes

The average intensity over species, $U^{(i)}(z,\vec{\Omega})$, can be decomposed into the direct and diffuse components, according to the pattern of incoming solar radiation, Eq. (6), namely

$$U^{(i)}(z,\vec{\Omega}) = \frac{f_{\mathrm{dir}}(\vec{\Omega}_0)}{|\mu(\vec{\Omega}_0)|}\,U_\delta^{(i)}(z)\,\delta(\vec{\Omega}-\vec{\Omega}_0) + U_d^{(i)}(z,\vec{\Omega}). \tag{21}$$

Substituting this decomposition into Eq. (20) and collecting terms, which contain the Dirac's delta function, $\delta(\vec{\Omega}-\vec{\Omega}_0)$, we will get system of N equations for the direct component of $U^{(i)}(z,\vec{\Omega})$,

$$U_\delta^{(i)}(z) + \frac{1}{|\mu(\vec{\Omega}_0)|}\sum_j \int_0^z \mathrm{d}\xi K^{(i,j)}(z,\xi,\vec{\Omega}_0)\,\sigma^{(j)}(\vec{\Omega}_0)\,U_\delta^{(j)}(\xi) = 1. \tag{22}$$

The remaining terms constitute the system of N equations for the diffuse component of $U^{(i)}(z,\vec{\Omega})$:

$$\begin{cases} U_{\mathrm{d}}^{(i)}(z,\vec{\Omega}) + \frac{1}{|\mu(\vec{\Omega})|}\sum_j \int_0^z \mathrm{d}\xi K^{(i,j)}(z,\xi,\vec{\Omega})\,\sigma^{(j)}(\vec{\Omega})\,U_d^{(j)}(\xi,\vec{\Omega}) \\ = \frac{1}{|\mu(\vec{\Omega})|}\sum_j \int_0^z \mathrm{d}\xi K^{(i,j)}(z,\xi,\vec{\Omega})\,S^{(j)}(\xi,\vec{\Omega}) + U_0^{(i)}(z,\vec{\Omega},\vec{\Omega}_0), \quad \mu<0, \\ U_d^{(i)}(z,\vec{\Omega}) + \frac{1}{|\mu(\vec{\Omega})|}\sum_j \int_z^H \mathrm{d}\xi K^{(i,j)}(z,\xi,\vec{\Omega})\cdot\sigma^{(j)}(\vec{\Omega})\,U_d^{(j)}(\xi,\vec{\Omega}) \\ = \frac{1}{|\mu(\vec{\Omega})|}\sum_j \int_z^H \mathrm{d}\xi K^{(i,j)}(z,\xi,\vec{\Omega})\,S^{(j)}(\xi,\vec{\Omega}) + U_H^{(i)}(z,\vec{\Omega},\vec{\Omega}_0), \quad \mu>0, \end{cases} \tag{23}$$

where,

$$S^{(j)}(\xi,\vec{\Omega}) = \int_{4\pi} \mathrm{d}\vec{\Omega}'\sigma_S^{(j)}(\vec{\Omega}'\to\vec{\Omega})\,U_d^{(j)}(\xi,\vec{\Omega}'), \tag{24}$$

$$U_0^{(i)}(z,\vec{\Omega},\vec{\Omega}_0) = \frac{f_{\rm dir}(\vec{\Omega}_0)}{|\mu(\vec{\Omega})\cdot\mu(\vec{\Omega}_0)|}\sum_j \int_0^z {\rm d}\xi K^{(i,j)}(z,\xi,\vec{\Omega})\cdot\sigma_S^{(j)}(\vec{\Omega}_0\to\vec{\Omega})\,U_\delta^{(j)}(\xi) + [1-f_{\rm dir}(\vec{\Omega}_0)]\,d(\vec{\Omega},\vec{\Omega}_0), \tag{25}$$

$$U_H^{(i)}(z,\vec{\Omega},\vec{\Omega}_0) = \frac{f_{\rm dir}(\vec{\Omega}_0)}{|\mu(\vec{\Omega})\,\mu(\vec{\Omega}_0)|}\sum_j \int_z^H {\rm d}\xi K^{(i,j)}(z,\xi,\vec{\Omega})\,\sigma_S^{(j)}(\vec{\Omega}_0\to\vec{\Omega})\,U_\delta^{(j)}(\xi) + U^{(i)}(H,\vec{\Omega}), \tag{26}$$

The average intensity over total space of a horizontal plane, $\bar{I}(z,\vec{\Omega})$, can be decomposed similarly to $U^{(i)}(z,\vec{\Omega})$, namely

$$\bar{I}(z,\vec{\Omega}) = \frac{f_{\rm dir}(\vec{\Omega}_0)}{|\mu(\vec{\Omega}_0)|}\,\bar{I}_\delta(z)\,\delta(\vec{\Omega}-\vec{\Omega}_0) + \bar{I}_d(z,\vec{\Omega}). \tag{27}$$

Substituting Eqs. (21) and (27) into Eq. (18) and collecting terms with the Dirac's Delta function and remaining terms, we obtain the equations for the direct and diffuse components of $\bar{I}(z,\vec{\Omega})$, respectively:

$$\bar{I}_\delta(z) = 1 - \frac{1}{|\mu(\vec{\Omega}_0)|}\sum_j \int_0^z {\rm d}\xi p^{(j)}(\xi)\,\sigma^{(j)}(\vec{\Omega}_0)\,U_\delta^{(j)}(\xi), \tag{28}$$

$$\begin{cases} \bar{I}_{\rm d}(z,\vec{\Omega}) = -\frac{1}{|\mu(\vec{\Omega})|}\sum_j \int_0^z {\rm d}\xi p^{(j)}(\xi)\,\sigma^{(j)}(\vec{\Omega})\,U_{\rm d}^{(j)}(\xi,\vec{\Omega}) \\ \quad + \frac{1}{|\mu(\vec{\Omega})|}\sum_j \int_0^z {\rm d}\xi p^{(j)}(\xi)\,S^{(j)}(\xi,\vec{\Omega}) + U_0^{(i)}(z,\vec{\Omega},\vec{\Omega}_0), \quad \mu<0, \\ \bar{I}_d(z,\vec{\Omega}) = -\frac{1}{|\mu(\vec{\Omega})|}\sum_j \int_z^H {\rm d}\xi p^{(j)}(\xi)\,\sigma^{(j)}(\vec{\Omega})\,U_{\rm d}^{(j)}(\xi,\vec{\Omega}) \\ \quad + \frac{1}{|\mu(\vec{\Omega})|}\sum_j \int_z^H {\rm d}\xi p^{(j)}(\xi)\,S^{(j)}(\xi,\vec{\Omega}) + U_H^{(i)}(z,\vec{\Omega},\vec{\Omega}_0), \quad \mu>0, \end{cases} \tag{29}$$

where $S^{(j)}(\xi,\vec{\Omega})$, $U_0^{(i)}(z,\vec{\Omega},\vec{\Omega}_0)$ and $U_H^{(i)}(z,\vec{\Omega},\vec{\Omega}_0)$ are defined by Eqs. (24)–(26).

3.4. Absorptance

The terms of energy conservation law (canopy albedo, absorptance and transmittance) and mean intensities ($\bar{I}(z,\vec{\Omega})$ and $U^{(i)}(z,\vec{\Omega})$), derived according to the stochastic approach, follow the general rules for the BS- and S- problems, Eqs. (7) and (8). The equation for absorptance has special features as it explicitly accounts for the contribution of different species, characterized by different optical properties. Taking into account the definition of absorptance and Eq. (17), the absorptance of the multi-species vegetation canopy is

$$\begin{aligned} A &\equiv \frac{1}{S_R}\int\int_{V\times 4\pi} {\rm d}\vec{r}\,{\rm d}\vec{\Omega}(1-\omega(\vec{r}))\,\sigma(\vec{r},\vec{\Omega})\,I(\vec{r},\vec{\Omega}) \\ &= \frac{1}{S_R}\int_0^H {\rm d}z\int_{4\pi}{\rm d}\vec{\Omega}\int_{\pi R^2}{\rm d}x\,{\rm d}y\sum_j \chi^{(j)}(\vec{r})\,(1-\omega^{(j)})\,\sigma^{(j)}(\vec{\Omega})\,I(\vec{r},\vec{\Omega}) \\ &= \sum_j (1-\omega^{(j)})\int_0^H {\rm d}z\int_{4\pi}{\rm d}\vec{\Omega}p^{(j)}(z)\,\sigma^{(j)}(\vec{\Omega})\,U^{(j)}(z,\vec{\Omega}). \end{aligned} \tag{30}$$

Taking into account Eqs. (30) and (7c), we can evaluate the contribution of the BS- and S- absorptances of different species to the total canopy absorptance:

$$A \approx \sum_j A_{\rm BS}^{(j)} + \frac{\rho_{\rm soil}}{1-\rho_{\rm soil}\,R_{\rm S}}\,T_{\rm BS}\,A_{\rm S}^{(j)}. \tag{31}$$

3.5. Conditional pair-correlation function of mixture of species

The critical parameters of the SMRT equations are two stochastic moments of a canopy structure: the probability of finding species, $p^{(i)}$ (Eq. (11)), and the conditional pair-correlation of species, $K^{(i,j)}$ (Eq. (13)). The following three classes of canopy structure can be identified: (a) non-ordered/chaotic mixture of species and gaps or TM; (b) ordered mixture of species without gaps; (c) ordered mixture of species with gaps. The canopy structure (order/chaoticity) is controlled by the conditional pair-correlation of species, $K^{(i,j)}$, while amount of gaps is controlled by the probability of finding species $p^{(i)}$. In the general case, $K^{(i,j)}$ satisfies the following symmetry condition:

$$p^{(i)}(z)\,K^{(i,j)}(z,\xi,\vec{\Omega}) \equiv S_R \cap T_z^{(i)}\,\frac{S_R \cap T_z^{(i)} \cap T_\xi^{(j)}}{S_R \cap T_z^{(i)}} = S_R \cap T_\xi^{(j)}\,\frac{S_R \cap T_\xi^{(j)} \cap T_z^{(i)}}{S_R \cap T_\xi^{(j)}}$$
$$\equiv p^{(j)}(\xi)\,K^{(j,i)}(\xi,z,-\vec{\Omega}). \tag{32}$$

The additional properties of $K^{(i,j)}$ in the special cases are as follows. In the case of TM there is no correlation between phytoelements of different species, and therefore, $K^{(i,j)}$ simplifies:

$$K^{(i,j)}(z,\xi,\vec{\Omega}) = \frac{q^{(i,j)}(z,\xi,\vec{\Omega})}{p^{(i)}(z)} = \frac{p^{(i)}(z)\,p^{(j)}(\xi)}{p^{(i)}(z)} = p^{(j)}(\xi). \tag{33}$$

In the case of ordered species without gaps, $K^{(i,j)}$ satisfies the following two constraints:

$$\sum_j K^{(i,j)}(z,\xi,\vec{\Omega}) \equiv \sum_j \frac{S_R \cap T_z^{(i)} \cap T_\xi^{(j)}}{S_R \cap T_z^{(i)}} = 1, \tag{34}$$

$$\sum_i p^{(i)}(z)\,K^{(i,j)}(z,\xi,\vec{\Omega}) \equiv \sum_i \frac{S_R \cap T_z^{(i)}}{S_R}\,\frac{S_R \cap T_z^{(i)} \cap T_\xi^{(j)}}{S_R \cap T_z^{(i)}} = p^{(j)}(\xi), \tag{35}$$

if and only if,

$$\sum_j p^{(j)}(z) \equiv \sum_j \frac{S_R \cap T_z^{(j)}}{S_R} = 1.$$

Finally, consider the case of ordered mixture of species with gaps. We developed the conditional pair-correlation function according to the theory of stochastic geometry [20]. This approach was utilized recently to derive the conditional pair-correlation function for single species [17]. In this research, we extend derivations to a mixture of multiple species (Appendix 2). The derivations are based on the following assumptions about 3D stochastic canopy structure: (a) tree species are modeled as identical cylinders; (b) distribution of the tree centers follows stationary Poisson point process [20]. Under the above assumptions, the conditional pair-correlation function is as follows:

$$K^{(i,j)}(\Delta) = \begin{cases} [2p^{(i)} - 1 + (1-p^{(i)})^{2-\Xi(\Delta)/\pi a^2}]/p^{(i)}, & i = j, \\ 1 - (1-p^{(i)})^{1-\Xi(\Delta)/\pi a^2}, & i \neq j, \end{cases} \tag{36a}$$

where

$$\Xi(\Delta) = 2a^2\left[\arccos\left(\frac{\Delta}{2a}\right) - \frac{\Delta}{2a}\sqrt{1-\left(\frac{\Delta}{2a}\right)^2}\right]\Theta(2a-\Delta). \tag{36b}$$

In the above equations, parameter "a" denotes a tree radius, $p^{(i)}$ is the canopy depth independent probability of finding species, $\Theta(x)$ is the Heaviside step function (cf. Appendix 2), and Δ is the horizontal distance of correlation:

$$\Delta = |(z-\xi)\,\tan(\vec{\Omega})|. \tag{36c}$$

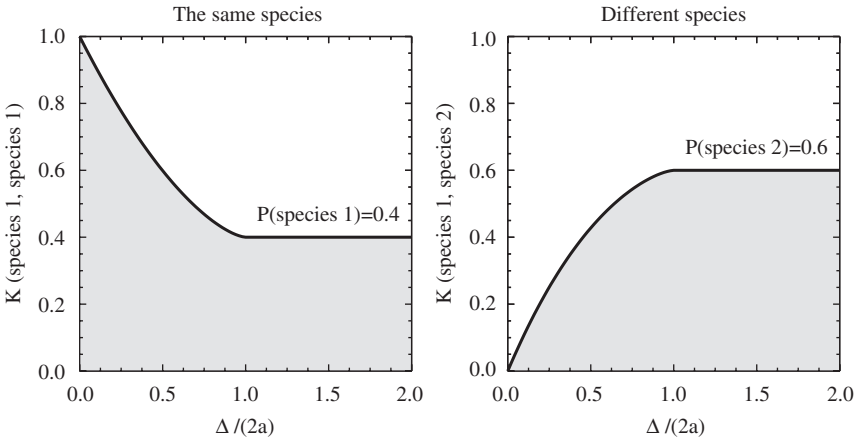

Fig. 2. The conditional pair-correlation function, $K(i,j)$, of the SMRT model as function of horizontal distance of correlation, Δ, normalized by three diameter, 2a. The parameters are as follows: two species with probabilities $p^{(1)} = 0.4$ and $p^{(2)} = 0.6$; tree radius $a = 0.15$; canopy height $H = 1$.

The conditional pair-correlation function for two species is shown in Fig. 2. In the case of the same species, correlation decreases as distance increases. This corresponds to increasing probability of one of the points being out of the same crown as distance increases. In the case of different species, correlation increases as distance increases. This corresponds to increasing probability of two points to be located in different crowns of different species with increasing distance. In the case of short distances, within-species correlation is 1, while between-species correlation is 0. In the case of large distances, correlation between any species is vanishing and $K^{(i,j)}$ converges to $p^{(i)}$. Both limiting cases are intuitively expected and captured by the proposed model.

4. Analytical analysis

In this section, we demonstrate results of analytical analysis of the SMRT equations for the three cases of canopy structure (cf. Section 3.5): (a) non-ordered mixture of species and gaps (TM); (b) ordered mixture of species without gaps; (c) ordered mixture of species with gaps.

4.1. Turbid medium

In the case of non-ordered mixture of vegetation species and gaps (TM) $K^{(i,j)}$ is reduced to $p^{(j)}$ (cf. Eq. (33)). In this case Eq. (20) is equivalent to Eq. (18) and $\bar{I}(z,\vec{\Omega}) = U^{(i)}(z,\vec{\Omega})$ for $i = 1,N$, which implies no variation of the radiation fluxes between different species. Lack of variation between species fluxes is a consequence of the lack of spatial gradient of structure in a TM: the same proportion of different species occupies each spatial location at particular canopy depth. Note, that the impact of gaps on radiation fluxes in the TM approach is limited to re-scaling of LAI:

$$\mathrm{LAI}^{(\text{with gaps})} = \mathrm{LAI}^{(\text{no gaps})} \sum_j p^{(j)}.$$

Also note, that in the case of a TM, the system of N mixture equations with species-dependent optical properties is reduced to a single equation with "effective" optical properties,

$$X^{(\text{effective})}(z) = \sum_j X^{(j)}(z)\, p^{(j)}(z), \tag{37}$$

where X corresponds to σ, σ_S, $(1-\omega)\cdot\sigma$, d_L, etc. As mentioned before (cf. Section 1), approach of "effective" optical properties was already implemented in the scaling scheme of the radiation block of the Command Land Model and the MODIS LAI algorithm. Such approach is valid only for non-ordered canopy (TM) and may lead to a bias in evaluation of the radiation field of a natural structured mixture (cf. Section 5).

4.2. Ordered mixture without gaps

Next, consider the special case of ordered mixture of vegetation species with no gaps between them. This case is not equivalent to a TM, because spatial heterogeneity is characterized not only by ordered composition of vegetation clumps and gaps, but also by ordered composition of different species ($K^{(i,j)} \neq p^{(j)}$). In this special case some constraints for the SMRT equations can be derived. In the following derivations, we assume

$$\sum_j p^{(j)}(z) = 1. \tag{38}$$

For simplicity, we perform derivations for direct component of radiation over species, $U_\delta^{(i)}(z)$. Multiplying Eq. (22) by $p^{(i)}(z)$ and performing summation over index "i", we have

$$\sum_i p^{(i)}(z)\, U_\delta^{(i)}(z) + \frac{1}{|\mu(\vec{\Omega}_0)|} \sum_i \sum_j \int_0^z \mathrm{d}\xi p^{(i)}(z)\, K^{(i,j)}(z,\xi,\vec{\Omega}_0)\, \sigma^{(j)}(\vec{\Omega}_0)\, U_\delta^{(j)}(\xi) = \sum_i p^{(i)}(z).$$

Taking into account Eqs. (35) and (38), the above equation is reduced to

$$\sum_j p^{(j)}(z)\, U_\delta^{(j)}(z) + \frac{1}{|\mu(\vec{\Omega}_0)|} \sum_j \int_0^z \mathrm{d}\xi p^{(j)}(\xi)\, \sigma^{(j)}(\vec{\Omega}_0)\, U_\delta^{(j)}(\xi) = 1. \tag{39}$$

Note, that Eq. (39) does not uniquely specify the solution, rather it provides a general constrain for a family of solutions with different $K^{(i,j)}$. Comparing Eqs. (39) and (28) we have

$$\bar{I}_\delta(z) = \sum_j p^{(j)}(z)\, U_\delta^{(j)}(z). \tag{40a}$$

Applying the above derivation technique to Eqs. (23) and (29), we will derive similar equation for total intensity (both direct and diffuse components), namely

$$\bar{I}(z,\vec{\Omega}) = \sum_j p^{(j)}(z)\, U^{(j)}(z,\vec{\Omega}). \tag{40b}$$

The above equation can be easily satisfied in the special case of the TM model, as radiation over all species is the same. However this equation is applicable to a more general case of ordered mixture of species with species-dependant fluxes (cf. Sections 4.4 and 5).

4.3. Radiation over gaps

Next, consider the general case of ordered species with gaps. In the framework of the SMRT model gaps can be treated as a special type of vegetation species with $\sigma = \sigma_s = 0$ and $d_L = 0$. The equation for the mean intensity over gaps, $U^{(\mathrm{gap})}(z,\vec{\Omega})$, can be derived as follows. Consider system of $N+1$ species, i.e., N vegetation species and 1 "species" of gaps, such that

$$\sum_j p^{(j)}(z) + p^{(\mathrm{gap})}(z) = 1.$$

According to Eq. (40b), formulated for the above $N+1$ species,

$$\bar{I}(z,\vec{\Omega}) = p^{(\mathrm{gap})}\, U^{(\mathrm{gap})}(z,\vec{\Omega}) + \sum_j p^{(j)}(z)\, U^{(j)}(z,\vec{\Omega}). \tag{41}$$

Combining the above two equations, we will get expression for $U^{(\mathrm{gap})}(z,\vec{\Omega})$, namely

$$U^{(\mathrm{gap})}(z,\vec{\Omega}) = \frac{1}{1-\sum_j p^{(j)}(z)} \left[\bar{I}(z,\vec{\Omega}) - \sum_j p^{(j)}(z)\, U^{(j)}(z,\vec{\Omega}) \right]. \tag{42a}$$

Note, that in the case of the TM (cf. Section 4.1), Eq. (42a) is reduced to

$$U^{(\mathrm{gap})}(z,\vec{\Omega}) = \bar{I}(z,\vec{\Omega}) = U^{(j)}(z,\vec{\Omega}). \tag{42b}$$

The derived equations for the mean radiation over gaps have important implications for LAI retrievals from field measurements of radiation by a range of commercial optical instruments, including LAI-2000, AccuPAR, TRAC, etc. [21]. Measurements are performed over gaps and retrievals are performed according to the TM model, which does not differentiate between fluxes over gaps and vegetation species (Eq. (42b)). In reality, radiation fluxes over individual vegetation species and gaps may show substantial variation. To achieve better accuracy, retreival technique of the standard optical instruments needs to be reformulated in terms of stochastic equations.

4.4. Uncollided radiation

Next, consider the SMRT equations in the limiting case of uncollided radiation. This case can serve as an approximation for VIS wavelengths, where absorption is large and scattering is limited. In the following, we will compare derivations for TM and ordered medium, to further clarify impact of canopy structure on radiation regime. To simplify derivations we assume that incoming radiation is purely direct (SZA $= 0^0$) and probabilities of species do not depend on canopy depths, i.e., $p^{(i)}(z) \equiv p^{(i)}$. First, consider the TM case. Recall, that in this case $K^{(i,j)} = p^{(i)}$ (cf. Section 4.1) and system of Eq. (22) for direct radiation, $U_\delta^{(i)}$, is reduces to a single equation:

$$U_\delta(z) + \sum_j p^{(j)}\,\sigma^{(j)} \int_0^z \mathrm{d}\xi\, U_\delta(\xi) = 1.$$

The solution of the above equation is

$$U_\delta(z) \equiv I_\delta(z) \equiv T(z) = \exp\left(-\sum_j p^{(j)}\,\sigma^{(j)}\, z\right), \tag{43a}$$

where $T(z)$ denotes canopy transmittance at depth z. The canopy absorptance can also be analytically evaluated (cf. Eq. (30) for $\omega^{(j)} = 0$, $j = 1,N$) as follows:

$$A = \sum_j p^{(j)}\sigma^{(j)} \int_0^H \mathrm{d}\xi\, U_\delta(\xi) = 1 - \exp\left(-\sum_j p^{(j)}\,\sigma^{(j)}\, H\right). \tag{43b}$$

Next, consider the case of ordered species composition. In the following derivation we will use the conditional pair-correlation, as defined by Eqs. (36a) and (36b). According to these equations and the specified assumptions, $K^{(i,j)} = 1$, if $i = j$, and $K^{(i,j)} = 0$, if $i \neq j$. In this case, Eq. (22) reduces from a system of equations to a set of independent equations for individual species ($i = [1,N]$), namely

$$U_\delta^{(i)}(z) + \sigma^{(i)} \int_0^z \mathrm{d}\xi\, U_\delta^{(i)}(\xi) = 1.$$

The solution of each equation above depends on parameters of individual species, not whole mixture,

$$U_\delta^{(i)}(z) = \exp(-\sigma^{(i)} z).$$

The Eq. (28) for mean intensity in this case is reduces to

$$\bar{I}_\delta(z) \equiv T(z) = 1 - \sum_j p^{(j)}\,\sigma^{(j)} \int_0^z \mathrm{d}\xi\, U_\delta^{(j)}(\xi) = 1 - \sum_j p^{(j)}\,[1 - \exp(-\sigma^{(j)} z)]. \tag{44a}$$

The canopy absorptance is calculated as follows:

$$A = \sum_j p^{(j)}\,\sigma^{(j)} \int_0^H \mathrm{d}\xi\, U_\delta^{(j)}(\xi) = \sum_j p^{(j)}\,[1 - \exp(-\sigma^{(j)}\, H)]. \tag{44b}$$

Compare canopy transmittance for the turbid (Eq. (43a)) and ordered (Eq. (44a) medium. As LAI (or canopy depth, H) is increasing, the canopy transmittance converges to 0 in the case of the TM, and to a gap probability in the case of the ordered medium. The ordered medium case provides a realistic description of the radiation regime, as it accounts for radiation streaming through gaps without interaction with vegetation, such that portion of the sunlit area at the ground is equal to the gap probability. Next, compare absorptance for the turbid (Eqs. (43b)) and ordered (44b) medium. As LAI increases the canopy absorptance converges to 1 in the case of TM and to cumulative probability of all species in the case of the ordered medium. Again, the case of ordered medium provides a more realistic description of the radiation regime, as only the portion of photons, traveling through leaves can be absorbed. Finally, comparison of the structure of equations for absorptance and transmittance indicates that in the case of TM species interact significantly, while in the case of structured medium they are radiatively decoupled. Overestimation of species radiative coupling in the TM model take place because this model neglects spatial clumping of species.

4.5. Linear mixing assumption

Multiple land algorithms utilized for estimation of land cover mixture from coarse resolution satellite data rely on the empirical model of linear mixture of species (cf. Section 1). Under this assumption, canopy spectral reflectance of a mixed pixel is expressed as a linear combination of canopy spectral reflectances of pure species [1,2]. The linear mixture model ignores species radiative coupling. This coupling in a natural canopy is caused by multiple scattering, that is, after interaction with phytoelements of the first species, photon is scattered into another species.

The SMRT model can be reduced to the linear mixture model, and allows analysis of empirical assumptions of the latter. Indeed, according to Eq. (41), mean radiation over mixed pixel, $\bar{I}(z,\vec{\Omega})$, is equal to a weighted average of the radiation fields over pure species, $U^{(i)}(z,\vec{\Omega})$, and gaps, $U^{(\mathrm{gap})}(z,\vec{\Omega})$. However, $U^{(i)}(z,\vec{\Omega})$ are coupled though system of Eq. (20). In order to derive the linear mixture model from SMRT model one needs to break the coupling, that is, set to 0 the conditional pair-correlation function for different species, $\mathrm{K}^{(\mathrm{i,j})} = 0$, when $i \neq j$. This assumption apparently violates the basic geometry constraints on $K^{(i,j)}$ (i.e., Eqs. (34) and (35) in the case of no gaps), and intuitively one may expect that non-physical decoupling may result in the violation of energy conservation law. However this is not true. To demonstrate this, consider system of Eq. (18), where $U^{(i)}(z,\vec{\Omega})$ are derived from Eq. (20), formulated for single species 'i' (more precisely, mixture of species 'i' and gaps). Eq. (18) can be rewritten in a short form as

$$\begin{cases} \bar{I}^{(\mathrm{total})}(z) - \bar{I}^{(\mathrm{total})}(0) = \sum\limits_j \Psi^{(j)}(z), & \mu < 0, \\ \bar{I}^{(\mathrm{total})}(z) - \bar{I}^{(\mathrm{total})}(H) = \sum\limits_j \Psi^{(j)}(z), & \mu > 0, \end{cases} \tag{45}$$

where $\Psi^{(j)}(z)$ corresponds to the terms under the sign of sum over species in Eq. (18), $\bar{I}^{(\mathrm{total})}(z)$ is the mean intensity over whole mixture at height z, and $\bar{I}^{(\mathrm{total})}(0)(\bar{I}^{(\mathrm{total})}(H))$ corresponds to boundary value at the canopy top (bottom). The $\Psi^{(j)}(z)$ functions are available from Eq. (18), formulated for single species 'j':

$$\begin{cases} \bar{I}^{(j)}(z) - \bar{I}^{(j)}(0) = \Psi^{(j)}(z), & \mu < 0, \\ \bar{I}^{(j)}(z) - \bar{I}^{(j)}(H) = \Psi^{(j)}(z), & \mu > 0. \end{cases} \tag{46}$$

Combining Eqs. (45) and (46) we have

$$\begin{cases} \bar{I}^{(\mathrm{total})}(z) = \sum\limits_j [\bar{I}^{(j)}(z) - \bar{I}^{(j)}(0)] + \bar{I}^{(\mathrm{total})}(0), & \mu < 0, \\ \bar{I}^{(\mathrm{total})}(z) = \sum\limits_j [\bar{I}^{(j)}(z) - \bar{I}^{(j)}(H)] + \bar{I}^{(\mathrm{total})}(H), & \mu > 0. \end{cases} \tag{47}$$

Next, we integrate Eq. (47) over lower and upper hemispheres to evaluate reflectances, R, and transmittances, T, and substitute the results into the energy conservation law (Eq. (8a)),

$$\begin{aligned} R+A+(1-\rho)T &= \sum_j [R^{(j)}-R^{(j)}(H)] + R^{(\mathrm{total})}(H) + \sum_j A^{(j)} + (1-\rho)\sum_j [T^{(j)}-T^{(j)}(0)] + (1-\rho)T^{(\mathrm{total})}(0), \\ &= \sum_j [R^{(j)}+A^{(j)}+(1-\rho)T^{(j)}] - \sum_j [R^{(j)}(H)+(1-\rho)T^{(j)}(0)] + R^{(\mathrm{total})}(H) + (1-\rho)T^{(\mathrm{total})}(0), \\ &= n - \sum_j [R^{(j)}(H)+(1-\rho)T^{(j)}(0)] + R^{(\mathrm{total})}(H) + (1-\rho)T^{(\mathrm{total})}(0). \end{aligned} \tag{48}$$

In the last transformation we utilized the fact that the energy conservation law is valid for the single-species problem, that is,

$$R^{(j)} + A^{(j)} + (1-\rho)T^{(j)} = 1.$$

Therefore, for the special case of the BS-problem, we have

$$F^{(j)}(0) = F^{(\mathrm{total})}(0) = 1, \quad F^{(j)}(H) = F^{(\mathrm{total})}(H) = 0, \quad \rho = 0, \Rightarrow \quad R + A + (1-\rho)T = 1,$$

and for the S-problem,

$$F^{(j)}(0) = F^{(\mathrm{total})}(0) = 0, \quad F^{(j)}(H) = F^{(\mathrm{total})}(H) = 1, \quad \rho = 0, \quad \Rightarrow R + A + (1-\rho)T = 1.$$

Finally, from the validity of the energy conservation law for BS- and S- problems it follows the validity of this law for the total problem (this can be shown by combining Eq. (7) and (8)). Therefore, while radiative decoupling of vegetation species is physically meaningless, it is still a mathematically valid exercise and may describe RT processes in some other medium.

To summarize, the results of this and previous sections indicate that the linear mixture model ignores, while TM overestimates species radiative coupling compared to a realistic description of the SMRT model. The effect of radiation coupling will be further studied numerically in Section 5.

5. Numerical analysis

The SMRT model was implemented numerically using successive orders of scattering approximations (cf. Appendix 3). In the following, we numerically investigate features of the SMRT model by comparison to the TM model. Both cases were implemented with the same set of stochastic equations and input parameters, except the conditional pair-correlation function: Eq. (36) was used to implement the SMRT model, and Eq. (33) for the TM model (cf. Section 3.5). To understand the overall merits of the new model, consider radiation fluxes as function of canopy depth, as shown in Fig. 3. The SMRT model differentiates between radiation fluxes over individual species, gaps, and whole mixture (corresponding to mean intensities $U^{(i)}$, $U^{(\mathrm{gap})}$ and $\bar{I}$). The TM model provides no distinction between the above fluxes (cf. Section 4.1). According to the SMRT model, variation of the fluxes between individual vegetation species is relatively smaller compared to difference in fluxes between vegetation and gaps. Also note, that limitations of the TM model result in a bias (both overestimation and underestimation) in estimation of mean fluxes over whole mixture compared to the SMRT simulations (compare fluxes over whole mixture). Detailed analysis of the impact of various parameters on the SMRT and TM models simulations is presented with six case studies below (Figs. 4–9).

First, consider impact of solar zenith angle (SZA) on canopy albedo, absorptance and transmittance as function of LAI, as simulated with the SMRT and TM models at red and NIR wavelengths (Fig. 4). The simulations were performed with SZA of 0° and 60°. Two vegetation species with gaps were used: $p^{(1)} = 0.2$, $p^{(2)} = 0.3$, $p^{(\mathrm{gap})} = 0.5$. The complete set of parameters is presented in the figure caption. In the case of simulations for SZA $= 0^\circ$, the SMRT model predicts lower albedo, substantially lower absorptance and substantially higher transmittance compared to the TM model. However, at SZA $= 60^\circ$ both models demonstrate quite similar results. The key physical explanation for the difference between the SMRT and TM simulations at SZA $= 0^\circ$ is that the SMRT model accounts for radiation streaming through gaps without

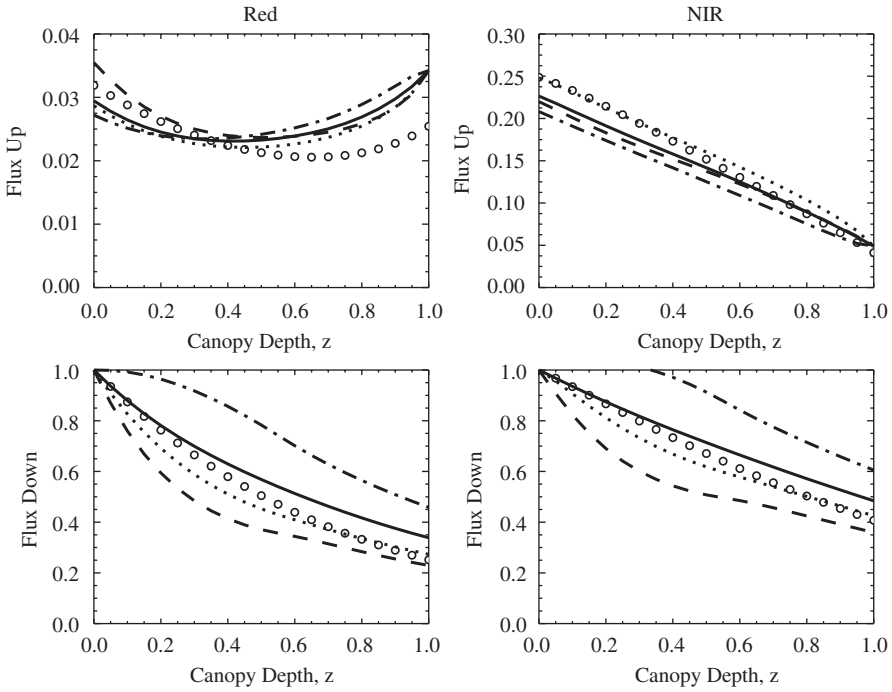

Fig. 3. Comparison of vertical profiles of up and down radiation fluxes as simulated by the TM and SMRT models for mixture of two species and gaps. The SMRT model captures spatial variation of fluxes between species 1 (red, dashed line), species 2 (red, dotted line), and gaps (red, dash-dot line) and also evaluates average flux over whole mixture (black, solid line). The TM model estimates only average flux over whole mixture (black, dotted line). The models parameters are as follows: $p^{(1)} = 0.40$, $p^{(2)} = 0.20$; $d_L^{(1)} = 4$, $d_L^{(2)} = 6$; $\omega^{(1)}(\text{red}) = 0.12$, $\omega^{(2)}(\text{red}) = 0.20$, $\omega^{(1)}(\text{NIR}) = 0.90$, $\omega^{(2)}(\text{NIR}) = 0.60$; $\rho_{\text{soil}}(\text{red}) = \rho_{\text{soil}}(\text{NIR}) = 0.10$; direct incoming flux, SZA $= 15^\circ$.

interaction with vegetation. This explains results for absorptance and transmittance. Albedo is lower in the case of the SMRT compared to the TM model, because in the former case a dark soil is better exposed through gaps in a relatively bright vegetation (compare ρ_{soil} and ω). Next, note that the numerical simulations for absorptance and transmittance at red wavelength closely follow analytical expressions, derived for uncollided radiation for SZA $= 0^\circ$ (cf. Section 4.4). For instance, in the case of the SMRT model canopy transmittance for high LAI approaches to 0.5 according to numerical simulations, which match $1-(p^{(1)}+p^{(2)})$, according to analytical analysis (Eq. (44a)). In contrast, in the case of the TM model, transmittance converges to 0 both according to numerical and analytical results (Eq. (43a)). Next, we explain results for SZA $= 60^\circ$. In this case the effect of radiation streaming is negligible: even if photon enters canopy through a gap, it will be intercepted by a lateral surface of a tree foliage. Mathematically, the reasoning is as follows: as angle is increasing, effective distance between vegetation elements, Δ, is increasing (cf. Eq. (36)), which results in convergence of the conditional pair-correlation function for ordered species to one for non-ordered species (cf. Fig. 2).

Second, consider the impact of soil reflectance on the radiation quantities (Fig. 5). Set of parameters for this case study was similar to the previous one, except SZA is fixed and equal to 0°, while two soil albedos (0 and 1) were used. Note the special feature of the canopy albedo for high LAI: in the case of the TM model, albedo converges to a single value, independently from soil albedo, while such convergence does not exist in the case of the SMRT model. This is another effect, associated with radiation streaming through gaps. Next, consider results for absorptance. Canopy absorptance is increasing with increasing soil albedo, and such effect is more pronounced for the SMRT model. The physical explanation for this is that some portion of the total radiation can stream through the gaps to the canopy bottom without being absorbed. If soil is bright, this radiation is bounced back and receives a second chance to be absorbed by a canopy. However, if soil is dark, this mechanism is vanishing. Finally, consider results for transmittance. In the case of red wavelength, soil albedo has virtually no effects on transmittance both for the TM and SMRT models. In the case of NIR wavelength,

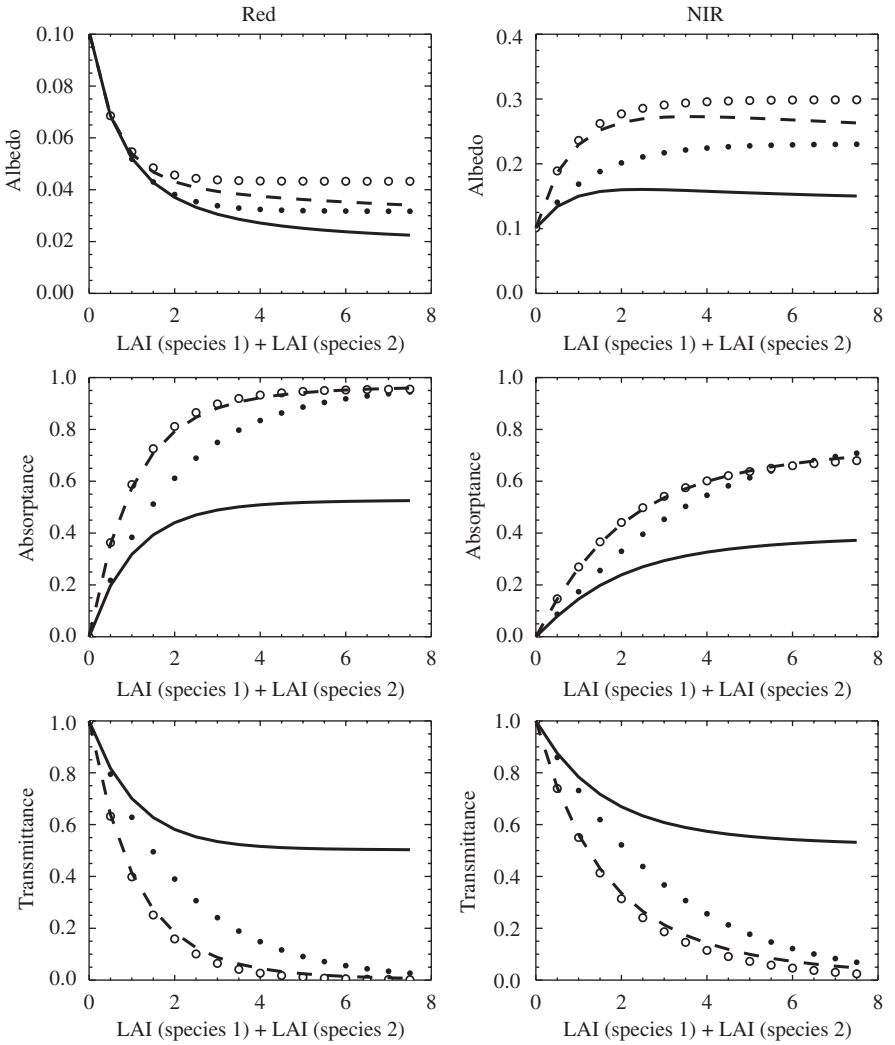

Fig. 4. Impact of SZA on canopy albedo, absorptance and transmittance, as evaluated with the TM (dots) and SMRT (solid lines) models. Runs for direct incoming flux with SZA $= 0^\circ$ and $= 60^\circ$ are shown in black and red, respectively. The other parameters are as follows: $p^{(1)} = 0.20$, $p^{(2)} = 0.30$; $d_L^{(1)} = d_L^{(2)} = [0.0–16.0]$; $\omega^{(1)}(\text{red}) = 0.12$, $\omega^{(2)}(\text{red}) = 0.20$, $\omega^{(1)}(\text{NIR}) = 0.90$, $\omega^{(2)}(\text{NIR}) = 0.60$; $\rho_{\text{soil}}(\text{red}) = \rho_{\text{soil}}(\text{NIR}) = 0.10$.

higher soil reflectance results in a higher transmittance and this effect is enhanced in the SMRT simulations due to radiation streaming through gaps.

Third, consider the impact of species composition on a radiation regime (Fig. 6). Here we used two species with optical properties roughly corresponding to broadleaf (species 1) and needle leaf (species 2) forests, which have substantial contrast both at red and NIR wavelengths. The probability of each species ($p^{(1)}$ and $p^{(2)}$) was varying from 0 up to 0.6, under restriction, that total probability of all species is constant through the simulations, i.e., $p^{(1)} + p^{(2)} = 0.6 =$ fixed. Thus, radiation regime was evaluated for all possible combinations of two species under significant amount of gaps, $p^{(\text{gap})} = 0.4 =$ fixed. Our results indicate, that both the TM and SMRT models simulate continuous, fairly large variation of canopy albedo, absorptance and transmittance with respect to species composition. However, the TM model introduces a significant bias in the estimation of the above parameters due to ignoring canopy structure. Finally, note that variations of canopy albedo, absorptance and transmittance with respect to species compositions are quite close to linear at red wavelength, but demonstrate fairly large deviation from linearity at NIR wavelength. Note that

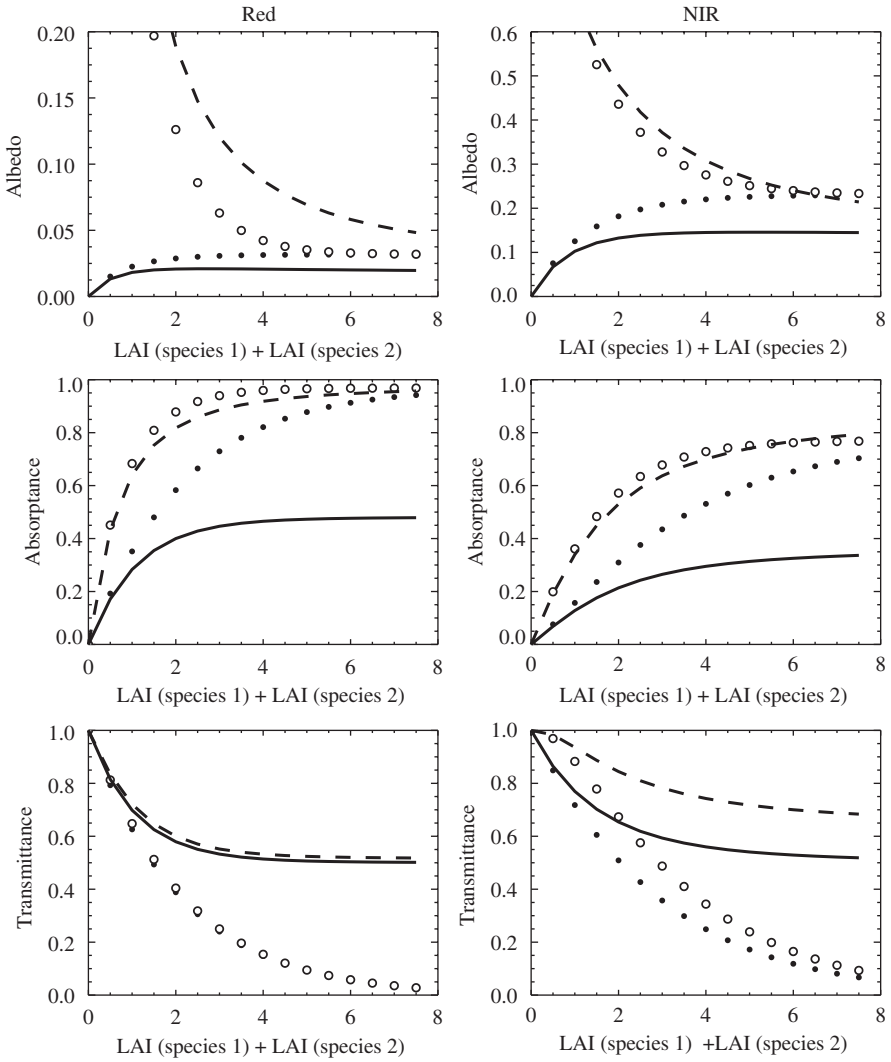

Fig. 5. Impact of soil reflectance on canopy albedo, absorptance and transmittance, as evaluated with the TM (dotted lines) and SMRT (solid lines) models. Runs with soil reflectance $\rho_{soil}(red) = \rho_{soil}(NIR) = 0.0$ and $= 1.0$ are shown in black and red, respectively. The other parameters are as follows: $p^{(1)} = 0.20$, $p^{(2)} = 0.30$; $d_L^{(1)} = d_L^{(2)} = [0.0–16.0]$; $\omega^{(1)}(red) = 0.12$, $\omega^{(2)}(red) = 0.20$, $\omega^{(1)}(NIR) = 0.90$, $\omega^{(2)}(NIR) = 0.60$; direct incoming flux, SZA $= 0^\circ$.

linearity for absorptance with respect to species composition can be seen in Eqs. (43b) and (44b) in the case of high LAI.

Fourth, consider the role of gaps in a radiation regime (Fig. 7). Simulations were performed for two species under constrain that the probabilities of both species are equal and its sum is varying between 0 (only gaps) and 1 (only vegetation). The SMRT model is not equivalent to the TM model even in the limiting case of no gaps (cf. Section 4.2). Results for canopy albedo are as follows. Albedo at red wavelength is decreasing as gaps are replaced with vegetation, because albedo of leaves was selected to be comparable to soil albedo, however, when more leaves are introduced, they trap radiation, scattered within canopy, more efficiently. Also, canopy albedo for the TM and SMRT models are approximately equal at red wavelength. However, at NIR wavelength albedo is increasing with decreasing amount of gaps, and the TM model predicts higher albedo compared to the SMRT model. The physical reason for this is that at NIR wavelength leaves are brighter then soil, and therefore, increasing amount of leaves will increase albedo. Additionally, vegetation gas of the TM model efficiently covers soil, compared to discontinuous canopy with gaps in the SMRT model, which results

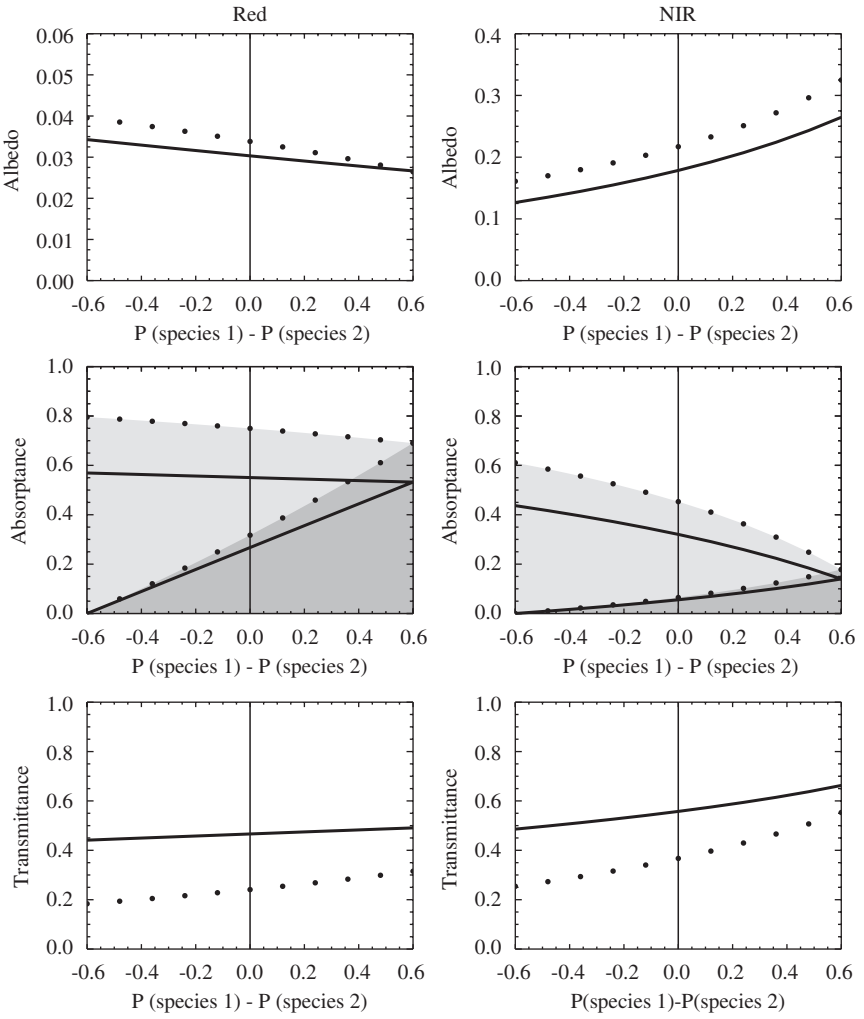

Fig. 6. Impact of species composition on canopy albedo, absorptance and transmittance, as evaluated with the TM (dots) and SMRT (solid lines) models for the case of mixture of two species. The models parameters are as follows: $p^{(1)}+p^{(2)}=0.60$; $d_L^{(1)}=4.0$, $d_L^{(2)}=6.0$; $\omega^{(1)}(\text{red})=0.12$, $\omega^{(2)}(\text{red})=0.20$, $\omega^{(1)}(\text{NIR})=0.90$, $\omega^{(2)}(\text{NIR})=0.60$; $\rho_{\text{soil}}(\text{red})=\rho_{\text{soil}}(\text{NIR})=0.10$; direct incoming flux, SZA $=0^0$.- Shaded areas correspond to absorptance of individual species.

in further enhancement of albedo in the TM model compared to the SMRT model. Next, the simulations indicate that overestimation of absorptance by the TM model compared to the SMRT model is directly proportional to the gap fraction/clumping of species. Finally, results for canopy transmittance indicate that as amount of gaps is decreasing, transmittance, evaluated by the SMRT model converges to one for the TM model.

In the fifth case study, we probed deeper special case of mixture of species without gaps (Fig. 8). Intuitively, in the case of no gaps, ordered mixture of species is quite close to non-ordered mixture (TM). In this simulation we addressed two questions: (a) When ordered mixture of species is important? (b) Why gaps significantly perturb radiation field of ordered mixture of species? As mentioned earlier, key feature of vegetation structure, which differentiates between ordered and non-ordered cases is a presence of spatial gradient of optical properties of a medium (such as leaf albedo, density of LAI, etc.). If the medium is ordered, the spatial gradient of the optical properties should be significant enough to modify the radiation regime of the SMRT simulations with respect to the TM simulations. Optical properties of gaps constitute especially large contrast to ones of any vegetation species. This explains special role of gaps in the SMRT simulations.

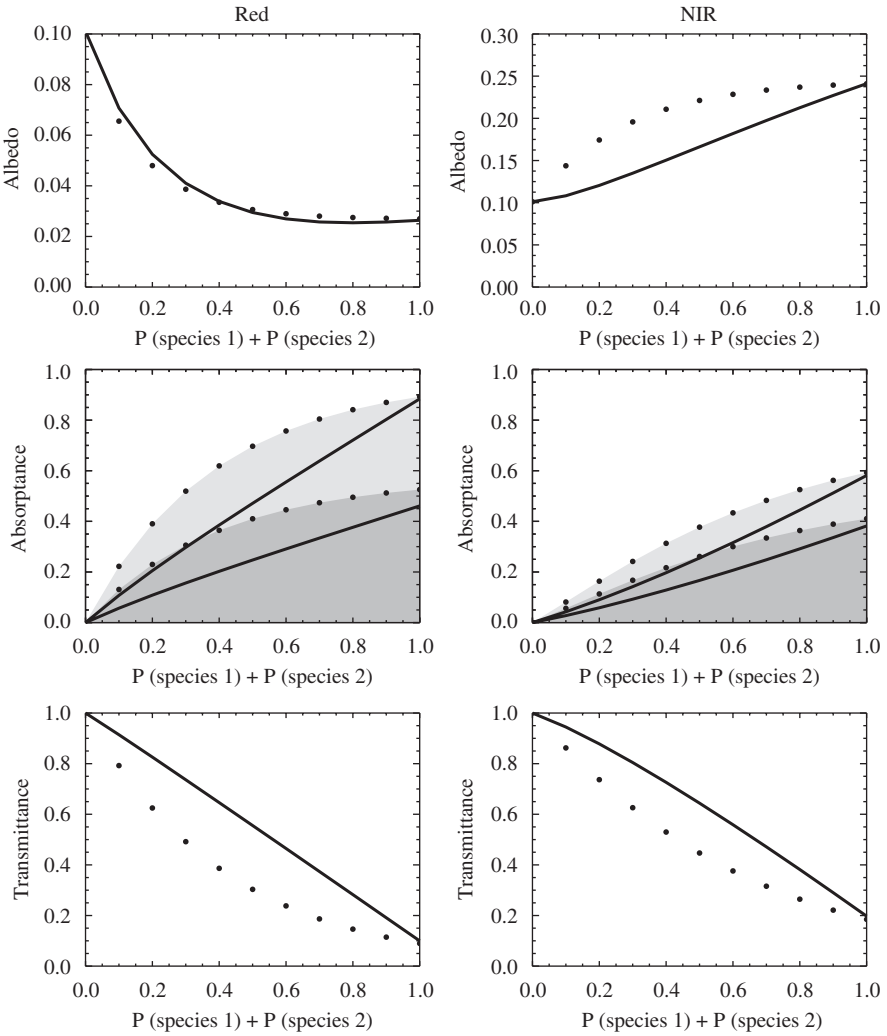

Fig. 7. Impact of gaps on canopy albedo, absorptance and transmittance, as evaluated with the TM (dotted lines) and SMRT (solid lines) models for the case of mixture of two species. The models parameters are as follows: $p^{(1)} = p^{(2)} = [0.0–0.5]$; $d_L^{(1)} = 4.0$, $d_L^{(2)} = 6.0$; $\omega^{(1)}(\text{red}) = 0.12$, $\omega^{(2)}(\text{red}) = 0.16$, $\omega^{(1)}(\text{NIR}) = 0.80$, $\omega^{(2)}(\text{NIR}) = 0.70$; $\rho_{\text{soil}}(\text{red}) = \rho_{\text{soil}}(\text{NIR}) = 0.10$; direct incoming flux, SZA $= 0^\circ$. Shaded areas correspond to absorptance of individual species.

The variation of the optical properties of vegetation species is as follows: leaf albedo may vary by factor of 2 in majority of cases, while variation in the foliage area volume density may be arbitrary large. Our test runs (not presented here) indicate no significant difference between the SMRT and TM simulations as function of variations of leaf albedo for typical vegetation canopies. Simulations for two species with varying foliage area volume density ($d_L^{(1)}$ and $d_L^{(2)}$) indicate significant bias in the estimation of absorptance by the TM model with respect to the SMRT model when $d_L^{(2)}/d_L^{(1)} = 0$, no difference when $d_L^{(2)}/d_L^{(1)} = 1$, and increasing bias with respect to increasing contrast in the foliage area volume density of species (Fig. 8). Note that the TM model introduces bias not only to total absorptance but also to the partitioning of total canopy absorptance between species.

Next, consider the sixth case study, demonstrating the effect of species interaction (Fig. 9). Here we evaluated the impact of LAI changes of species 2 on the absorptance of species 1. The LAI of species 2 was constructed according to two scenarios: (a) keep $p^{(2)}$ constant and vary $d_L^{(2)}$ (top two panels for red and NIR wavelengths); (b) keep $d_L^{(2)}$ constant and vary $p^{(2)}$ (lower panels). We also used two illumination conditions:

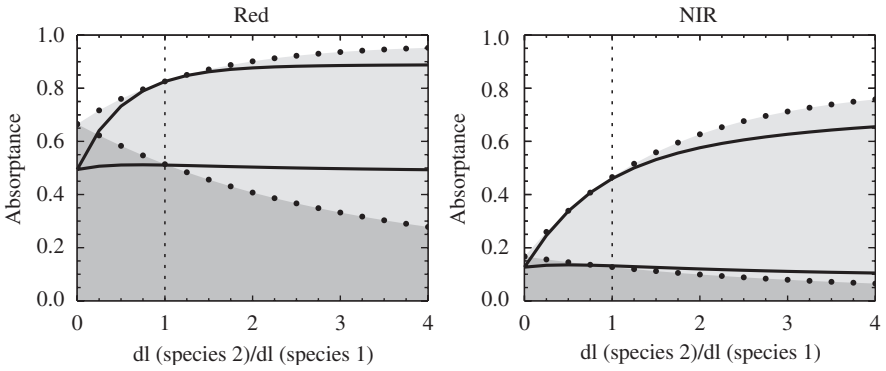

Fig. 8. Impact of species LAI density on partitioning of total absorptance between individual species, as evaluated with the TM (dotted lines) and SMRT (solid lines) models for the case of mixture of two species. The models parameters are as follows: $p^{(1)} = 0.4$, $p^{(2)} = 0.6$; $d_L^{(1)} = 4.0$, $d_L^{(2)} = [0.0–16.0]$; $\omega^{(1)}(\text{red}) = 0.12$, $\omega^{(2)}(\text{red}) = 0.20$, $\omega^{(1)}(\text{NIR}) = 0.90$, $\omega^{(2)}(\text{NIR}) = 0.60$; $\rho_{\text{soil}}(\text{red}) = \rho_{\text{soil}}(\text{NIR}) = 0.10$; direct incoming flux, SZA $= 0^\circ$. Shaded areas correspond to absorptance of individual species.

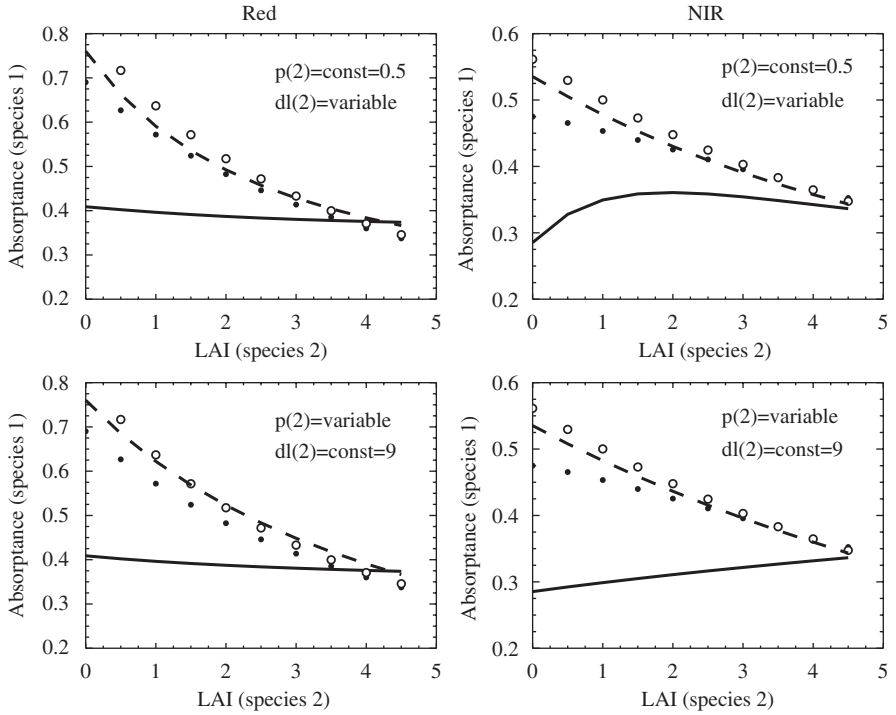

Fig. 9. Impact of species interaction on canopy absorptance, as evaluated with the TM (dotted lines) and SMRT (solid lines) models. Runs for direct (SZA $= 0^\circ$), and diffuse incoming fluxes are shown in black and red, respectively. The other parameters are as follows: $p^{(1)} = 0.4$, $p^{(2)} = 0.5$ or variable; $d_L^{(1)} = 6$, $d_L^{(2)} = 9$ or variable; $\omega^{(1)}(\text{red}) = 0.12$, $\omega^{(2)}(\text{red}) = 0.16$, $\omega^{(1)}(\text{NIR}) = 0.60$, $\omega^{(2)}(\text{NIR}) = 0.80$; $\rho_{\text{soil}}(\text{red}) = \rho_{\text{soil}}(\text{NIR}) = 0.1$.

purely direct incoming flux, SZA $= 0^\circ$; and purely diffuse incoming flux. The results indicate, that absorptance of species 1 decreases by factor of two both at red and NIR wavelengths as LAI of species 2 is changing from 0 to 4 in the case of the TM model under direct illumination. In contrast, the SMRT model predicts no significant variations in the absorptance of species 1 at red wavelength, and increase by about 15% in the case of NIR wavelength under direct illumination. In the case of diffuse illumination the SMRT and TM models predict similar interaction of species- decrease of the absorptance of the first species as LAI of the second is

increasing. This last result of this case study matches the results of the first case study: under diffuse illumination or low SZA, the simulations by both models converge. Overall, this last case study demonstrates that natural mixture of discontinuous species exhibit less radiative coupling compared to the TM approximation.

Our final comment is on the overall performance of the SMRT model. The SMRT code is computationally compact-CPU requirements are similar to those for the solution of 1D RT code [18]. Computational errors increase with increasing LAI, SZA, which is typical for majority of the RT models. Additional errors, specific to the SMRT, can be accumulated under the condition of large number of species with highly varying optical properties. In this study the performance of the model was not evaluated with respect to field measurements, as authors did not have access to the required set of structured parameters and radiation measurements of sufficiently high accuracy. The model validation should be performed within a separate study in the future. Nevertheless, confidence in the SMRT model performance should be drawn from the fact, that the mixture model extends the one for single species, which was extensively evaluated with field measurements and was utilized in multiple applications in the past [17,18,22–24].

6. Concluding remarks

In this research, we developed the SMRT model for simulation of radiation regime in a natural vegetation canopy with spatially varying optical properties. The new approach provides a general solution of the problem, which includes, as special cases, the major approximate solutions, including the linear mixture and TM mixture RT models. The SMRT model solves for the radiation quantities, direct input to remote sensing/climate applications: mean fluxes over mixture and over individual species. The canopy structure is parameterized in the SMRT model in terms of two stochastic moments: the probability of finding species and the conditional pair-correlation of species. The second moment is responsible for the 3D radiation effects, namely, radiation streaming through gaps without interaction with vegetation and variation of the radiation fluxes between different species. If the within- and between-species correlation is vanishing, the SMRT model reduces to the TM RT model. Namely, this situation is realized in the SMRT simulations under direct illumination with low SZA or diffuse illumination. If the between- (but not within-) species correlation is set to zero, the SMRT model reduces to the linear mixture model. The analysis of the SMRT simulations indicates that the variation of radiation fluxes between different species is proportional to the variation of optical properties of species (leaf albedo, density of foliage, etc.) Gaps introduce significant disturbance to the radiation regime in the mixed canopy as their optical properties constitute a major contrast to those of any vegetation species. Set of accurate field measurements on canopy structure and radiation is required to further assess performance of the SMRT model and to improve modeling of the pair-correlation function.

Acknowledgments

This research was supported by NASA MODIS contract NNG04HZ09C and Interdisciplinary Science (IDS) in the NASA Earth Science Enterprise grant G35C14G2. We thank the anonymous reviewer for stimulating discussion, helped to improve our analysis.

Appendix 1. Nomenclature

H	height of the canopy
$\vec{\Omega} = \{\Omega_x, \Omega_y, \Omega_z\}$	unit vector of solid angle
$\mu(\vec{\Omega})$	cosine of polar angle in direction $\vec{\Omega}$
$\delta(\vec{\Omega} - \vec{\Omega}_0)$	Dirac's delta function
$\chi^{(i)}(\vec{r})$	indicator function of species 'i' at spatial location $\vec{r}$
S_R	set/area of circle with radius R

$T_z^{(i)}$	set/area of horizontal plane at depth z, covered by species 'i'
$S_R \cap T_z^{(i)}$	common area of S_R and $T_z^{(i)}$
$p^{(i)}(z)$	probability of finding species 'i' at depth z
$K^{(i,j)}(z,\xi,\vec{\Omega})$	conditional probability of finding species 'j' at depth ξ, given species 'i' at depth z along direction $\vec{\Omega}$
$I(\vec{r},\vec{\Omega})$	radiation intensity, radiance at spatial point $\vec{r}$ and in direction $\vec{\Omega}$, normalized by extraterrestrial solar irradiance (sr^{-1})
$U^{(i)}(z,\vec{\Omega})$	mean radiation intensity over species 'i' at depth z (sr^{-1})
$\bar{I}(z,\vec{\Omega})$	mean radiation intensity over all space at depth z (sr^{-1})
$\omega(\lambda)$	spectral leaf albedo
$\rho_{\mathrm{soil}}(\lambda)$	soil hemispherical reflectance
L	leaf area index
$d_{\mathrm{L}}^{(i)}$	foliage area volume density of species 'i' ($\mathrm{m}^2\,\mathrm{m}^{-3}$)
$G(\vec{r},\vec{\Omega})$	mean projection of leaf normals in the direction $\vec{\Omega}$
$\frac{1}{\pi}\Gamma(\vec{r},\vec{\Omega}' \to \vec{\Omega})$	area scattering phase function (sr^{-1})
$\sigma_{\mathrm{S}}(\vec{\Omega}' \to \vec{\Omega})$	differential scattering cross-section ($\mathrm{m}^{-1}\,\mathrm{sr}^{-1}$)
$\sigma(\vec{\Omega})$	extinction coefficient ($\mathrm{m}^{-1}\,\mathrm{sr}^{-1}$)

Appendix 2. Derivation of the pair-correlation function

The approach to derive the pair-correlation function for a mixture of vegetation species is based on the theory of stochastic geometry [20], an analytical tool to describe statistical properties of patterns, encountered in many areas of science and technology. According to the concepts of stochastic geometry, spatial distribution of vegetation species can be modeled as a stationary Poisson point process: (a) total number of trees in the bounded study area follows Poisson distribution with intensity (stem density) d; (b) spatial distribution of trees is random. We further assume that all trees of particular species 'i' are identical vertical solids (volume obtained by rotating a curve, $r^{(i)}(z)$, about the vertical axis z).

Consider particular realization of canopy as schematically depicted in Fig. 1 of the main text. Pair-correlation function of mixture of species in a 3D canopy can be evaluated by taking cross-section of canopy at depth z and ξ and collapsing both planes along direction $\vec{\Omega}$. The collapsed planes are shifted by horizontal distance (cf. Fig. 1),

$$\Delta = |(z-\xi)\tan(\Omega)|. \tag{A.1}$$

Thus, evaluation of the pair–correlation function is reduced to calculation of the correlation of points in a 2D space of horizontal plane. The following derivations rely on the fact, that the event, featuring particular point, A, being within a tree of species 'i' is equivalent to the event of tree center, $C^{(i)}$, being within circle, $O(A, r^{(i)}(A))$, of radius $r^{(i)}(A)$, centered at this point. According to the stationary Poisson point process, the probability of the above event of finding species 'i' at depth z is

$$p^{(i)}(z) \equiv P(C^{(i)} \in O(A, r^{(i)}(A))) = 1 - \exp(-d\,\pi\,(r^{(i)}(z))^2). \tag{A.2}$$

Refer to Fig. A1 for the following derivations. First we derive the pair-correlation function for the same species. Consider Fig. A1(a), which shows two points, A and B, and respective neighborhood circles $O(A, r^{(i)}(A))$ and $O(B, r^{(i)}(B))$. Note that the circles may have intersection, $\Xi = O(A, r^{(i)}(A)) \cap O(B, r^{(i)}(B))$. Both points, A and B, belong to vegetation (meaning correlation) in two cases. In the first case, a single tree with a center, $C^{(i)}$, positioned in the intersection ,Ξ, i.e., $C^{(i)} \in \Xi$, will cover both points (single tree case). In the second case, both A and B can be inside of vegetation, if each is covered by a separate tree (two trees case). In order to ensure that second case is not reduced to the first one, each tree should not be positioned in the intersection area, Ξ, i.e., $C^{(i)} \in O(A, r^{(i)}(A))\Xi$ and $C^{(i)} \in O(B, r^{(i)}(B))\Xi$. The pair-correlation function for the

same species is the sum of probabilities, P, of the above two events:

$$q^{(i,i)}(A,B) = P(C^{(i)} \in \Xi) + [1 - P(C^{(i)} \in \Xi)]\, P(C^{(i)} \in O(A, r^{(i)}(A))\backslash\Xi)\, P(C^{(i)} \in O(B, r^{(i)}(B))\backslash\Xi) \tag{A.3a}$$

Next, we derive the pair-correlation function for different species. Consider Fig. (A1b), showing points A and B, surrounded by a neighborhood, occupied by species 'i' and 'j', respectively. If point B is surrounded by circle $O(B,\ r^{(j)}(B))$ for species 'j', point A should be surrounded by circle $O(A,\ r^{(i)}(A))$, reduced by the intersection area, Ξ, to preserve from covering point B. Therefore, the pair-correlation function for different species is

$$q^{(i,j)}(A,B) = P(C^{(i)} \in O(A, r^{(i)}(A))\backslash\Xi)\, P(C^{(j)} \in O(B, r^{(j)}(B))), \quad i \neq j. \tag{A.3b}$$

Note, that the above probabilities which involve intersection area can be evaluated similarly to Eq. (A.2), namely,

$$P(C^{(i)} \in \Xi) = 1 - \exp(-d\,\Xi), \tag{A.4a}$$

$$P(C^{(i)} \in O(A, r^{(i)}(A) - \Xi) = 1 - \exp(-d\,(\pi\,(r^{(i)}(z))^2 - \Xi))). \tag{A.4b}$$

Combining Eqs. (A.2), (A.3a, b) and (A.4a, b), we will get

$$q^{(i,i)}(z,\xi,\Delta) = p^{(i)}(z) + p^{(i)}(\xi) - 1 + [1 - p^{(i)}(\xi)]\,(1 - p^{(i)}(z))^{1-\Xi/\pi\cdot(r^{(i)}(z))^2} \tag{A.5a}$$

$$q^{(i,j)}(z,\xi,\Delta) = p^{(i)}(\xi)\,[1 - (1 - p^{(j)}(z))^{1-\Xi/\pi\cdot(r^{(i)}(z))^2}], \quad i \neq j \tag{A.5b}$$

The remaining unknown function, circles overlapping, Ξ, can be derived by referencing Fig. (A1c). Consider the general case of two circles with different radiuses, $r^{(j)}(\xi) > r^{(i)}(z)$, and centers, separated by distance Δ. Three situations of overlapping are possible: (a) small circle is inside of the larger one; (b) no overlapping between circles; (c) partial overlapping between circles. Geometrical analysis of each case will results in the following expression:

$$\Xi(\Delta) = \begin{cases} \pi \cdot (r^{(i)}(z))^2, & \text{if } r(\xi) - r(z) > \Delta, \ \text{(one inside of the other)}, \\ 0, \ \text{if } r(\xi) + r(z) \leqslant \Delta, \ \text{(no overlaping)}, \\ \alpha(r^{(i)}(z))^2 + \beta(r^{(j)}(\xi))^2 - \Delta\, r(\xi)\, \sin(\alpha), & \text{otherwise (overlaping)}, \end{cases}$$

Expression for Ξ in the case when $r^{(j)}(\xi) < r^{(i)}(z)$ can be derived from the above expression by interchanging $r^{(j)}(\xi)$ and $r^{(i)}(z)$.

Finally, consider special case of cylindrical trees, as referenced in the main text. In this case the geometry is simplified as follows:

$$r^{(i)}(z) = r^{(j)}(\xi) \equiv a,$$

$$p^{(i)}(z) \equiv p^{(i)}, \ \ i \in [1, N],$$

$$\alpha = \beta = \arccos\left(\frac{\Delta}{2a}\right),$$

$$\Xi(\Delta) = 2a^2 \left[\arccos\left(\frac{\Delta}{2a}\right) - \frac{\Delta}{2a}\sqrt{1 - \left(\frac{\Delta}{2a}\right)^2}\right] \Theta(2a - \Delta).$$

Above, $\Theta(x)$ is the Heaviside step function:

$$H(x) = \begin{cases} 1 & \text{if } x > 0, \\ 0 & \text{if } x < 0. \end{cases}$$

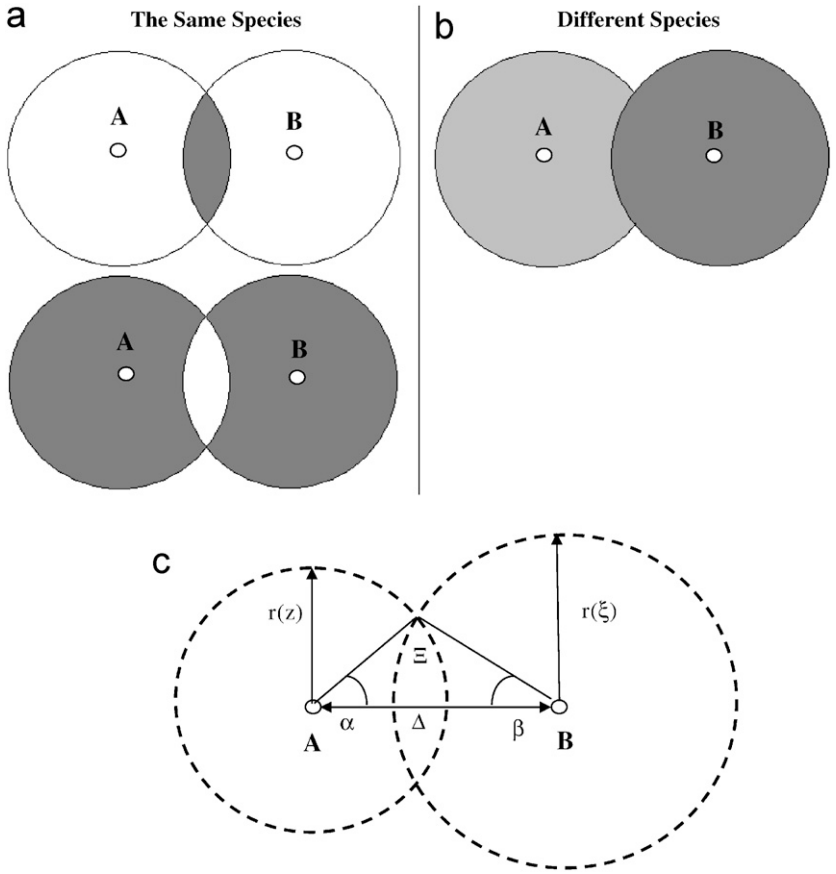

Fig. A1. The geometrical considerations in support of derivation of pair-correlation function. Correlation is evaluated for two points, A and B on horizontal plane. Panels (a) and (b) depict cases when correlation is achieved between the same species and different species respectively. Shaded areas of circles denote neighborhood of each point, where tree centers should be positioned to secure coverage of points A and B with vegetation. Panel (c) shows geometry in support of derivation of the area, Ξ, of intersection of two circles, separated by distance Δ.

Substituting the above equations into Eq. (A.5a,b), the pair-correlation function for the cylindrical trees is

$$q^{(i,i)}(\Delta) = 2p^{(i)} - 1 + (1 - p^{(i)})^{2-\Xi(\Delta)/\pi a^2}, \tag{A.6a}$$

$$q^{(i,j)}(\Delta) = p^{(i)}[1 - (1 - p^{(j)})^{1-\Xi(\Delta)/\pi a^2}], \quad i \neq j. \tag{A.6b}$$

Appendix 3. Numerical scheme of solution of SMRT

The numerical scheme of solution of the SMRT equations is an extension of the corresponding scheme for the SRT equations for single species [18]: single system of linear equations for singles species is expanded into N systems of linear equations for N species. According to Eqs. (28) and (29), the solution for the mean intensity over whole horizontal plane, $\bar{I}(z, \vec{\Omega})$, is just an integration of the mean intensities over individual species, $U^{(i)}(z, \vec{\Omega})$, $i = [1,N]$. Therefore, below we focus on the numerical scheme of solution for the direct and diffuse components of $U^{(i)}(z, \vec{\Omega})$: $U_{\mathrm{d}}^{(i)}(z, \vec{\Omega})$ (Eq. (23)) and $U_{\delta}^{(i)}(z)$ (Eq. (22)). The solution for the direct component requires solution of the parametric Volterra equation. Solution for the diffuse component is based on the successive orders of scattering approximations (SOSA) iterative method [25]; at each step of iterations we also need to solve the parametric Volterra equations. First, we outline SOSA method in application to a

mixture of species. The nth approximation to the solution for the diffuse component is

$$U_{\mathrm{d}}^{(i)}(z,\vec{\Omega})|_n = J_1^{(i)}(z,\vec{\Omega}) + J_2^{(i)}(z,\vec{\Omega}) + \ldots + J_n^{(i)}(z,\vec{\Omega}).$$

The functions $J_n^{(i)}(z,\vec{\Omega})$ are the solutions of the N system of the following parametric Volterra equations, derived from Eq. (23):

$$J_n^{(i)}(z,\vec{\Omega}) + \frac{1}{|\mu(\vec{\Omega})|}\sum_j \int_0^z \mathrm{d}\xi K^{(i,j)}(z,\xi,\vec{\Omega})\,\sigma^{(j)}(\vec{\Omega})\,J_n^{(j)}(\xi,\vec{\Omega}) = R_{n-1}^{(i)}(z,\vec{\Omega}), \quad \mu<0, \tag{B.1a}$$

$$J_n^{(i)}(z,\vec{\Omega}) + \frac{1}{|\mu(\vec{\Omega})|}\sum_j \int_z^H \mathrm{d}\xi K^{(i,j)}(z,\xi,\vec{\Omega})\,\sigma^{(j)}(\vec{\Omega})\,J_n^{(j)}(\xi,\vec{\Omega}) = R_{n-1}^{(i)}(z,\vec{\Omega}), \quad \mu>0. \tag{B.1b}$$

The right-hand side of Eq. (B.1) for $n=0$ is:

$$R_0^{(i)}(z,\vec{\Omega}) = \frac{f_{\mathrm{dir}}(\vec{\Omega}_0)}{|\mu(\vec{\Omega})\,\mu(\vec{\Omega}_0)|}\sum_j \int_0^z \mathrm{d}\xi K^{(i,j)}(z,\xi,\vec{\Omega})\,\sigma_S^{(j)}(\vec{\Omega}_0\to\vec{\Omega})\,U_\delta^{(j)}(\xi) + U^{(i)}(H,\vec{\Omega}), \quad \mu>0,$$

$$R_0^{(i)}(z,\vec{\Omega}) = \frac{f_{\mathrm{dir}}(\vec{\Omega}_0)}{|\mu(\vec{\Omega})\,\mu(\vec{\Omega}_0)|}\sum_j \int_z^H \mathrm{d}\xi K^{(i,j)}(z,\xi,\vec{\Omega})\,\sigma_S^{(j)}(\vec{\Omega}_0\to\vec{\Omega})\,U_\delta^{(j)}(\xi) + U^{(i)}(H,\vec{\Omega}), \quad \mu>0.$$

If $n>0$, the right-hand side of Eq. (B.1) is:

$$R_n^{(i)}(z,\vec{\Omega}) = \frac{1}{|\mu(\vec{\Omega})|}\sum_j \int_0^z \mathrm{d}\xi K^{(i,j)}(z,\xi,\vec{\Omega})\,S_n^{(j)}(\xi,\vec{\Omega}), \quad \mu<0 \text{ when } n\geqslant 1,$$

$$R_n^{(i)}(z,\vec{\Omega}) = \frac{1}{|\mu(\vec{\Omega})|}\sum_j \int_z^H \mathrm{d}\xi K^{(i,j)}(z,\xi,\vec{\Omega})\,S_n^{(j)}(\xi,\vec{\Omega}), \quad \mu>0 \text{ when } n\geqslant 1,$$

where

$$S_n^{(j)}(\xi,\vec{\Omega}) = \int_{4\pi} \mathrm{d}\vec{\Omega}'\,\sigma_S^{(j)}(\vec{\Omega}'\to\vec{\Omega})\,J_n^{(j)}(\xi,\vec{\Omega}').$$

The algorithm to solve the system of equations for $U_{\mathrm{d}}^{(i)}(z,\vec{\Omega})$ is as follows: (1) Find $U_\delta^{(i)}(z,\vec{\Omega})$ from the corresponding Volterra equation (Eq. (22)); (2) Evaluate $R_0^{(i)}(z,\vec{\Omega})$; (3) Solve the N systems of Volterra equations (Eqs. (B.1a) and (B.1b)) with $R_0^{(i)}(z,\vec{\Omega})$ and find $J_1^{(i)}(z,\vec{\Omega})$; (4) Evaluate $S_1^{(j)}(z,\vec{\Omega})$ with $J_1^{(i)}(z,\vec{\Omega})$; (5) Evaluate $R_1^{(i)}(z,\vec{\Omega})$; (6) Calculate $J_2^{(i)}(z,\vec{\Omega})$; (7) Repeat the following until desirable accuracy, $\max_i ||J_n^{(i)}(z,\vec{\Omega})|| \leqslant \varepsilon$, is achieved: (a) Evaluate $S_n^{(j)}(z,\vec{\Omega})$; (b) Calculate $R_n^{(i)}(z,\vec{\Omega})$; (c) Calculate $J_{n+1}^{(i)}(z,\vec{\Omega})$.

The scheme of solution for $U_{\mathrm{d}}^{(i)}(z,\vec{\Omega})$ and $U_\delta^{(i)}(z)$ according to Eqs. (22) and (B.1a, b) requires the corresponding scheme for the parametric Volterra equation of the following general form:

$$Q^{(i)}(z,\vec{\Omega}) + \frac{1}{|\mu(\vec{\Omega})|}\sum_j \int_0^z \mathrm{d}\xi K^{(i,j)}(z,\xi,\vec{\Omega})\,\sigma^{(j)}(\vec{\Omega})\,Q^{(j)}(\xi,\vec{\Omega}) = F^{(i)}(z,\vec{\Omega}). \tag{B.2}$$

Note that Eq. (B.2) corresponds to the system of N equations ($i=1,\ N$) and $\vec{\Omega}$ is a parameter of the parametric Volterra equation. The discrete form of Eq. (B.2) is as follows:

$$Q^{(i)}(k,\vec{\Omega}) + \frac{1}{|\mu(\vec{\Omega})|}\sum_j \sum_{\ell=1}^{k} K^{(i,j)}(k,\ell,\vec{\Omega})\,\sigma^{(j)}(\vec{\Omega})\,Q^{(j)}(\ell,\vec{\Omega}) = F^{(i)}(k,\vec{\Omega})$$

For the purpose of derivations let us rewrite the above equation as follows,

$$Q^{(i)}(k,\vec{\Omega}) + \frac{1}{|\mu(\vec{\Omega})|}\sum_j K^{(i,j)}(k,k,\vec{\Omega})\,\sigma^{(j)}(\vec{\Omega})\,Q^{(j)}(k,\vec{\Omega})$$
$$= F^{(i)}(k,\vec{\Omega}) - \frac{1}{|\mu(\vec{\Omega})|}\sum_j \sum_{\ell=1}^{k-1} K^{(i,j)}(k,\ell,\vec{\Omega})\,\sigma^{(j)}(\vec{\Omega})\,Q^{(j)}(\ell,\vec{\Omega})$$

This is a system of N linear equations in the form,

$$\widehat{\mathbf{A}}(k,\vec{\Omega}) \times \mathbf{Q}(k,\vec{\Omega}) = \mathbf{W}(k,\vec{\Omega}). \tag{B.3}$$

where $\widehat{\mathbf{A}}(k,\vec{\Omega})$ is an $N \times N$ matrix, and $Q(k,\vec{\Omega})$ and $W(k,\vec{\Omega})$ are N-elements vectors

$$\widehat{\mathbf{A}}^{(i,j)}(k,\vec{\Omega}) = \begin{cases} 1 + \dfrac{\sigma^{(i)}(\vec{\Omega})}{|\mu(\vec{\Omega})|}K^{(i,i)}(k,k,\vec{\Omega}) & \text{if } i = j, \\ \dfrac{\sigma^{(j)}(\vec{\Omega})}{|\mu(\vec{\Omega})|}K^{(i,j)}(k,k,\vec{\Omega}) & \text{if } i \neq j, \end{cases}$$

$$\mathbf{W}^{(i)}(k,\vec{\Omega}) = F^{(i)}(k,\vec{\Omega}) - \frac{1}{|\mu(\vec{\Omega})|}\sum_j \sum_{\ell=1}^{k-1} K^{(i,j)}(k,\ell,\vec{\Omega})\,\sigma^{(j)}(\vec{\Omega})\,Q^{(j)}(\ell,\vec{\Omega})$$

$$\mathbf{Q}^{(i)}(k,\vec{\Omega}) = Q^{(i)}(k,\vec{\Omega}).$$

The solution of Eq. (B.3) is derived iteratively starting with $k = 1$. At each step $\widehat{\mathbf{A}}(k,\vec{\Omega})$ is a known matrix, vector $W(k,\vec{\Omega})$ can be calculated from the previous step. The solution, $Q(k,\vec{\Omega}) = \widehat{\mathbf{A}}^{-1}(k,\vec{\Omega}) \times W(k,\vec{\Omega})$, can be derived by Gauss-Jordan, LU-decomposition or similar techniques for solving linear system of equations [26].

References

[1] DeFries RS, Townshend JRG, Hansen MC. Continuous fields of vegetation characteristics at the global scale 1-km resolution. J Geophys Res—Atmos 1999;104(D14):16911–23.

[2] Smith MO, Ustin SL, Adams JB, Gillespie AR. Vegetation in deserts: I. A regional measure of abundance from multispectral images. Remote Sens Environ 1990;31:1–26.

[3] Carpenter GA, Gopal S, Macomber S, Martens S, Woodcock CE. A neural network method for mixture estimation for vegetation mapping. Remote Sens Environ 1999;70:135–52.

[4] Shabanov NV, Lo K, Gopal S, Myneni RB. Sub-pixel burn detection in moderate resolution imaging spectroradiometer 500-m data with ARTMAP neural networks. J Geophys Res—Atmos 2005;110(D03111) 10292004JD005257.

[5] Ju J, Kolaczyk ED, Gopal S. Gaussian mixture discriminant analysis and sub-pixel land cover characterization in remote sensing. Remote Sens Environ 2003;84:550–60.

[6] McIver DK, Friedl MA. Using prior probabilities in decision-tree classification of remotely sensed data. Remote Sens Environ 2002;81:253–61.

[7] Borel C, Gerstl S. Nonlinear spectral mixing models for vegetative and soil surfaces. Remote Sens Environ 1994;47:403–16.

[8] Ray TW, Murray BC. Nonlinear spectral mixing in desert vegetation. Remote Sens Environ 1996;55:59–64.

[9] Tian Y, Dickinson RE, Zhou L, Zeng X, Dai Y, Myneni RB, et al. Comparison of seasonal and spatial variations of LAI/FPAR from MODIS and common land model. J Geophys Res—Atmos 2004;109(D1):D01103 10.1029/2003JD003777.

[10] Tian Y, Wang Y, Zhang Y, Knyazikhin Y, Bogaert J, Myneni RB. Radiative transfer based scaling of LAI/FPAR retrievals from reflectance data of different resolutions. Remote Sens Environ 2002;84:143–59.

[11] Vainikko GM. The equation of mean radiance in broken cloudiness. Trudy MGK SSSR, Meteorol Invest 1973;21:28–37 (in Russian).

[12] Vainikko GM. Transfer approach to the mean intensity of radiation in non-continuous clouds. Trudy MGK SSSR, Meteorol Invest 1973;21:38–57 (in Russian).

[13] Kasianov E. Stochastic radiative transfer in multilayer broken clouds. Part I: Markovian approach. JQSRT 2003;77(4):373–93.

[14] Titov GA. Statistical description of radiation transfer in clouds. J Atmos Sci 1990;47:24–38.

[15] Zuev VE, Titov GA. Atmospheric optics and climate. The series 'contemporary problems of atmospheric optics', vol. 9. Spector: Institute of Atmospheric Optics of Russian Academy of Sciences [in Russian].

[16] Pomraning GC. Linear kinetic theory and particle transport in stochastic mixtures. Series on advances in mathematics for applied sciences, vol. 7. Singapore: World Scientific; 1991.

[17] Huang D, Knyazikhin Y, Yang W, Wang W, Privette J, Deering D, et al. Stochastic transport theory for investigating the three-dimensional canopy structure from space measurements. Remote Sens Environ 2006; accepted June 2006.
[18] Shabanov NV, Knyazikhin Y, Baret F, Myneni RB. Stochastic modeling of radiation regime in discontinuous vegetation canopies. Remote Sens Environ 2000;74(1):125–44.
[19] Ross J. The radiation regime and architecture of plant stands. Hague: Dr. W. Junk Publishers; 1981.
[20] Stoyan D, Kendall WS, Mecke J. Stochastic geometry and its applications. Wiley series in probability and statistics, 2nd ed. New York: Wiley; 1995. p. 67–9.
[21] Breda NJJ. Ground-based measurements of leaf area index: a review of methods, instruments and current controversies. J Exp Bot 2003;64(392):2403–17.
[22] Kaufmann RK, Zhou L, Knyazikhin Y, Shabanov NV, Myneni RB, Tucker CJ. Effect of orbital drift and sensor changes on the time series of AVHRR vegetation index data. IEEE Trans Geosci Remote Sens 2000;38(6):2,584–97.
[23] Shabanov NV, Huang D, Yang W, Tan B, Knyazikhin Y, Myneni RB, et al. Analysis and optimization of the MODIS LAI and algorithm retrievals over broadleaf forests. IEEE Trans Geosci Remote Sens 2005;43(8):1855–65.
[24] Zhang Y, Shabanov NV, Knyazikhin Y, Myneni RB. Assessing information content of multiangle satellite data for mapping biomes. II Theory. Remote Sens Environ 2001;80:1–12.
[25] Myneni RB, Asrar G, Kanemasu ET. Light scattering in plant canopies: the method of successive orders of scattering approximations [SOSA]. Agric Forest Meteorol 1987;39:1–12.
[26] Press WH, Flannery BP, Teukolsky SA, Vetterling WT. Numerical recipes: the art of scientific computing. Cambridge: Cambridge University Press; 1986. p. 19–38.
[27] Foody GM. Relating the land-cover composition of mixed pixels to artificial neural network classification output. Photogrammetr Eng Remote Sens 1996;62:491–9.